# THE REPRESENTATION OF AUDITORY SPACE IN THE AUDITORY CORTEX OF ANESTHETIZED AND AWAKE MICE

## Matthias Gumbert
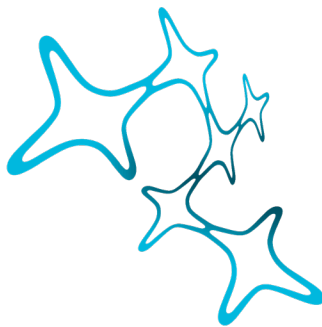
**Graduate School of Systemic Neurosciences**

**LMU Munich**

**Dissertation der**

**Graduate School of Systemic Neurosciences der**

**Ludwig-Maximilians-Universität München**

**20th December 2021**

Supervisor:

Prof. Dr. Benedikt Grothe
Division of Neurobiology, Department Biologie II
Ludwig-Maximilians-Universität München

First Reviewer:          Prof. Dr. Benedikt Grothe
Second Reviewer:         Prof. Dr. Michael Myoga
External Reviewer:       Prof. Dr. Dan Sanes

Date of Submission:      20/December/2021
Date of Defense:         25/March/2022

# ABSTRACT

The ability to localize sounds is of profound importance for animals, as it enables them to detect prey and predators. In the horizontal plane, sound localization is achieved by means of binaural cues, which are processed and interpreted by the ascending auditory pathway. The auditory cortex (AC), as its primary cortical relay station, has traditionally been thought to broadly and stationary represent the contralateral hemifield of auditory space. Because prior research on space representation in the mammalian AC heavily relied on anesthetized preparations, the manner in which anesthesia influences this representation has remained elusive. Performing chronic two-photon-calcium imaging in the AC of awake and anesthetized mice, I characterized the effects of anesthesia on auditory space representation. First, anesthesia was found to impair the spatial sensitivity of neurons. Second, anesthesia constantly suppressed the representation of frontal locations biasing spatial tuning to the contralateral side. In both conditions (awake and anesthetized), the population of neurons endured a stable representation of auditory space, while single-cell spatial tuning was found to be extremely dynamic. Importantly, under both conditions no evidence for a topographical map of auditory space was found. This study is the first to chronically probe spatial tuning in the AC and likewise the first to directly assess effects of anesthesia on single-cell spatial tuning and the population code emphasizing the need for a shift towards awake preparations.

# TABLE OF CONTENTS

# LIST OF FIGURES

# LIST OF ABBREVIATIONS

| | |
|---|---|
| AAV | adeno-associated virus |
| AC | auditory cortex |
| CA1 | primary cornu ammonis |
| $Ca^{2+}$ | calcium |
| CaM | calmodulin |
| dB | decibel |
| IC | inferior colliculus |
| ILD | interaural level difference |
| ITD | interaural time difference |
| GECI | genetically encoded calcium indicator |
| GFP | green fluorescent protein |
| LSO | lateral superior olive |
| MSO | medial superior olive |
| NL | nucleus laminaris |
| PPC | posterior parietal cortex |
| ROI | region of interest |
| SC | superior colliculus |
| SPL | sound pressure level |

x

# 1. INTRODUCTION

Audition is fundamental to secure an animal's survival and is the basis of a wide range of behaviors including communication, foraging and the identification of mating partners. Particularly, the localization of sounds is key for adequate responses and survival in a dynamic environment. Imagine crossing a busy street. Localization of automobiles allows you to assess if crossing that street is safe or not and in succession to initiate the appropriate behavior.

## 1.1. The anatomy of hearing and the ascending auditory pathway

Sounds are received as air-borne travelling waves. In mammals, these waves impinge on the animal's outer ear (*pinna*), travel through the ear canal and result in a deflection of the eardrum (*tympanum*). This causes the three middle ear bones (ossicles) to vibrate and in turn these vibrations are transmitted as amplified pressure waves within the cochlea's three fluid filled chambers. Between these three chambers resides the basilar membrane whose stiffness and width varies along its length. As a result, the pressure wave travels along the basilar membrane until it reaches the area of the basilar membrane that exhibits maximal resonance for the respective frequency of the pressure wave. The base of the basilar membrane resonates best with high frequencies, whereas low frequencies elicit maximal vibrations at the apex of the basilar membrane, thus creating a continuous map of frequency (tonotopy). The membrane's movement causes deflection of the stereocilia of the hair cells located on top of the basilar membrane. This causes hair cells to open their mechanical gated ion channels thus converting mechanical signals into membrane potential changes. Spiral ganglion cells then transmit the signal as action potentials via the auditory nerve to the cochlear nucleus. From the ventral cochlear nucleus neurons project to the superior olive subsequently relaying the signal to the lateral lemniscus and the inferior colliculus (IC). Additional pathways exist sparing the superior olive targeting the lateral lemniscus and the IC directly. The former is achieved by

axonal projections from the ventral cochlear nucleus. The latter by axonal projections from the dorsal cochlear nucleus. Upon convergence in the IC, the signal is relayed to the medial geniculate nucleus and afterwards to the AC (Grothe et al. 2010; Luo 2015).

## 1.2. The basics of spatial hearing

### 1.2.1. The cues used to extract spatial information from the environment

As has been described above only frequency information is mapped directly onto the basilar membrane being the sensory epithelium of the auditory system. Yet, no positional information is available at this level and must therefore be completely calculated within the brain.
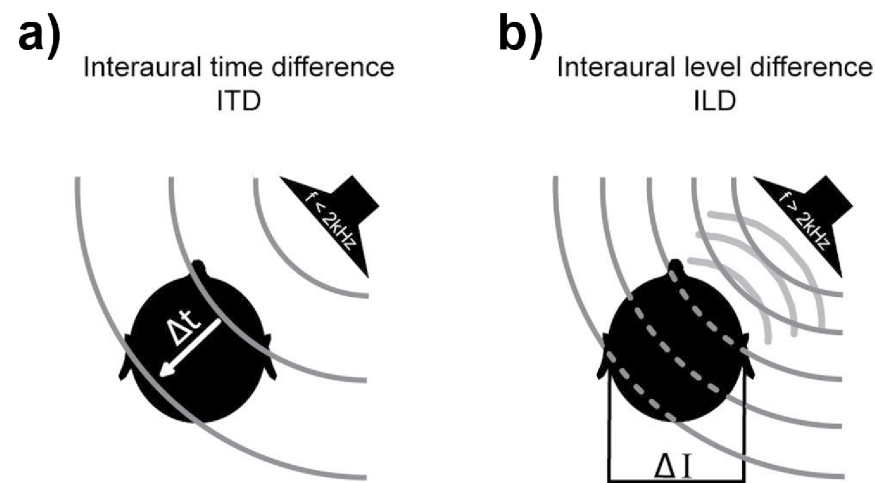


**Figure 1:** Binaural cues used to localize sound sources in the horizontal plane.
(a) Interaural time differences (ITDs) are used to decode the location of low-frequency sounds. Sounds lateral to the head impinge first on one ear and with some time delay at the other ear. These differences in elapsed time can be used to extract information about the location of the sound source.
(b) Interaural level differences (ILDs) are used to decode the location of high-frequency sounds. Sounds lateral to the head appear louder on one side of the head and fainter on the other side as the head exhibits a shadowing effect. These differences in loudness can be used to extract information about the location of the sound source.
Figure under Creative Commons license from Grothe and Pecka (2014).

Binaural cues are used to detect changes in the horizontal plane. First described by Rayleigh (1907), mammals have been shown to achieve sound localization by means of two different cues depending on interaural differences

(the duplex theory of sound localization). These are interaural time differences (ITDs) and interaural level differences (ILDs). ITDs are used to detect locations of low-frequency sounds. They appear if a sound source is not equidistant to both ears, causing differences in the arrival time at the two ears (Figure 1a). These differences are smallest (i.e. zero) for sounds originating in the front or back and increase with increasing stimulus laterality creating maximal ITDs at 90° to the left/right. High-frequency sounds (with wavelengths equal to or greater than head size width) are attenuated by the head causing differences in the sound intensity level at both ears with lower levels at the ear further away from the sound source thus creating ILDs (Figure 1b; Grothe et al. 2010). Due to their evolutionary heritage all terrestrial mammals exploit ILDs for sound localization, whereas relatively few make use of ITDs (see section 1.2.3; Grothe and Pecka 2014).

### 1.2.2. The Jeffress model and ITD detection in birds

ITDs require the accurate resolution of submillisecond differences in the arrival time at both ears. These differences are shorter than the average duration of an action potential (~1ms; Grothe and Pecka 2014) thereby challenging the auditory neural circuitry.

How then are the nuclei involved in ITD detection, capable of extracting these minute differences? In 1948 Jeffress (Jeffress 1948) published a visionary model of ITD processing (Figure 2) offering a simple and elegant solution. He postulated three major mechanisms that as a whole would allow a neural system to successfully detect ITDs. First, in this model ITD detection is supposed to be achieved via neuronal coincidence detectors that receive excitatory input from both ears. Second, delay lines varying in their axonal length from both ears tune these coincidence detectors to various best ITDs. Third, these coincidence detectors are supposed to be arranged in a systematic manner thus creating a topographical representation of ITDs.
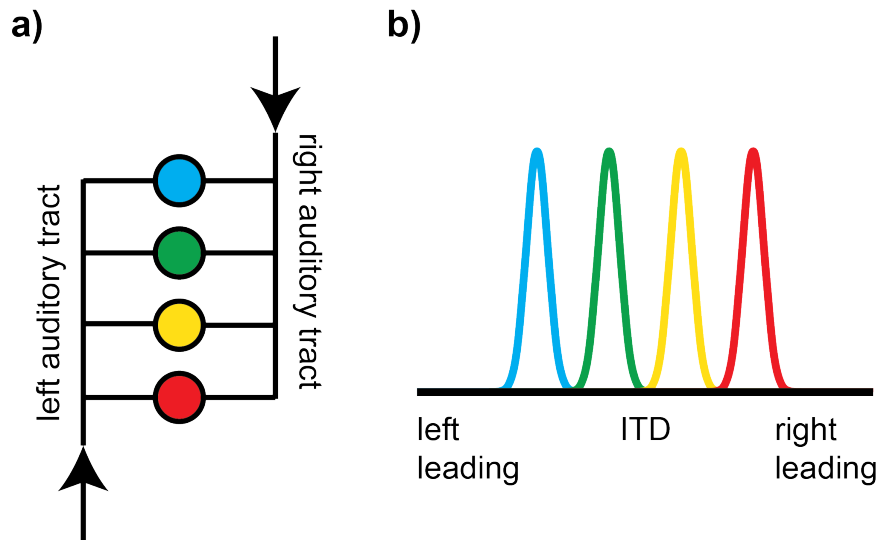
**Figure 2:** Schematic of ITD processing as proposed by Jeffress (1948).
(a) Systematic arrangement of coincidence detectors by means of excitatory delay lines. An ITD will cause excitation of one auditory tract first (e.g. left) and with some delay will excite the other tract (right). The signal travels along the delay lines until it converges at a coincidence detector, which is tuned to that specific ITD.
(b) ITD tuning curves of coincidence detector neurons. Due to their structured arrangement, coincidence detectors have clearly circumscribed ITD tuning functions.

Indeed, many of the model's assumptions have been found to be implemented in the auditory system of birds. Neurons within the nucleus laminaris (NL), the brain structure which enables ITD processing in the avian brain, receive binaural excitatory input. As predicted by Jeffress, these coincidence detector neurons are tuned to different ITDs due to orderly variations in axonal input length thus acting as delay lines (Parks and Rubel 1975; Carr and Konishi 1988; Overholt et al. 1992). Furthermore, the NL has been found to thereby create a topographical map of ITDs along its frequency bands (Carr and Konishi 1990). Maps of auditory space have also been reported in the seminal papers by Knudsen and Konishi for the avian analogue of the inferior colliculus (Knudsen and Konishi 1978) as well as for the optic tectum (superior colliculus analogue; Knudsen 1982). Together, these findings suggest that avian sound localization is achieved by means of a Jeffress-like system that relies on a labeled-line code.

### 1.2.3. Evolution of binaural hearing in birds and mammals

For a long time it has been assumed that mammals inherited their tympanic ears from birds (for review see Grothe et al. 2010). In succession the neural apparatus involved in sound localization has been hypothesized to be homologous in mammals and birds (see e.g. Masterton et al. 1967). Indeed, initial reports focusing on the neural implementation of ITD detection in mammals were in favor of a Jeffress-like system (Yin and Chan 1990; Smith et al. 1993; Joris et al. 1998; Beckius et al. 1999). Still, emerging evidence from the fossil record shattered the long standing idea of tympanic ear evolution. In the late 1990s Clack (1997) could show that in mammals and birds tympanic hearing evolved independently, yet around the same time in the Triassic. As a result, the neural mechanisms underlying auditory processing and binaural hearing cannot be considered to be homologues in birds and mammals but need to be studied separately. As I will discuss in the following paragraphs it is of utmost importance to consider the evolutionary pressure dominating the origin of spatial hearing in mammals and birds when developing models of spatial hearing.

A fundamental assumption of evolutionary theory is the idea that organisms adapt to their ecological niche (Darwin 1859). As dinosaurs were large in body and head size possessing only a single ossicle which limited their hearing range to low frequencies, they had to rely on ITD processing exclusively (Grothe and Pecka 2014). Birds as their descendants seemed to have expanded their hearing range only very little (Heffner and Heffner 2007). In contrast, early mammals possessed already three ossicles which presumably transmitted high frequencies best (Rosowski and Graybeal 1991). Furthermore, mammals probably made use of high frequency communication calls thus being acoustically separated from archosaurian predators (Grothe and Pecka 2014). The ability to predominantly perceive high frequencies in combination with their

small body and head size most likely had early mammals initially to rely on ILDs for sound localization. Only later changes in the hearing range or head size required the additional use of ITDs in some mammals including humans. Thus, evolving from a different ecological niche than birds, binaural hearing originally had to serve different purposes in mammals (escape behavior) and in avian ancestors (prey capture). Therefore, physical restrictions and evolutionary pressure created different means of sound localization in archosaurs (crocodiles and birds as recent representatives). Whereas, in archosaurs ITDs were the original cues used for sound localization, mammals incipiently relied on ILDs (for a comprehensive review on the evolution of spatial hearing see Grothe and Pecka 2014). As I will elaborate in the following sections, this has resulted in the development of different neural mechanisms for spatial hearing in mammals.

### 1.2.4. ITD and ILD detection in mammals

ITD processing in mammals occurs primarily at the medial superior olive (MSO) – the mammalian analogue to the avian NL. In contrast to birds, ITD computation in mammals relies on a delicate temporal integration of binaural excitatory and inhibitory inputs (Figure 3a; Grothe and Sanes 1993, 1994; Grothe 2003; Grothe et al. 2010; Grothe and Pecka 2014). MSO neurons usually have broad tuning functions increasing monotonically over a large range of azimuthal space peaking outside the range of physiological detectable ITDs (Figure 3b; Pecka et al. 2008; Grothe 2003; Grothe et al. 2010; Grothe and Pecka 2014). This suggests that mammals do not perform ITD computation by means of a neural circuitry as proposed by Jeffress (1948) but favor a different coding strategy.
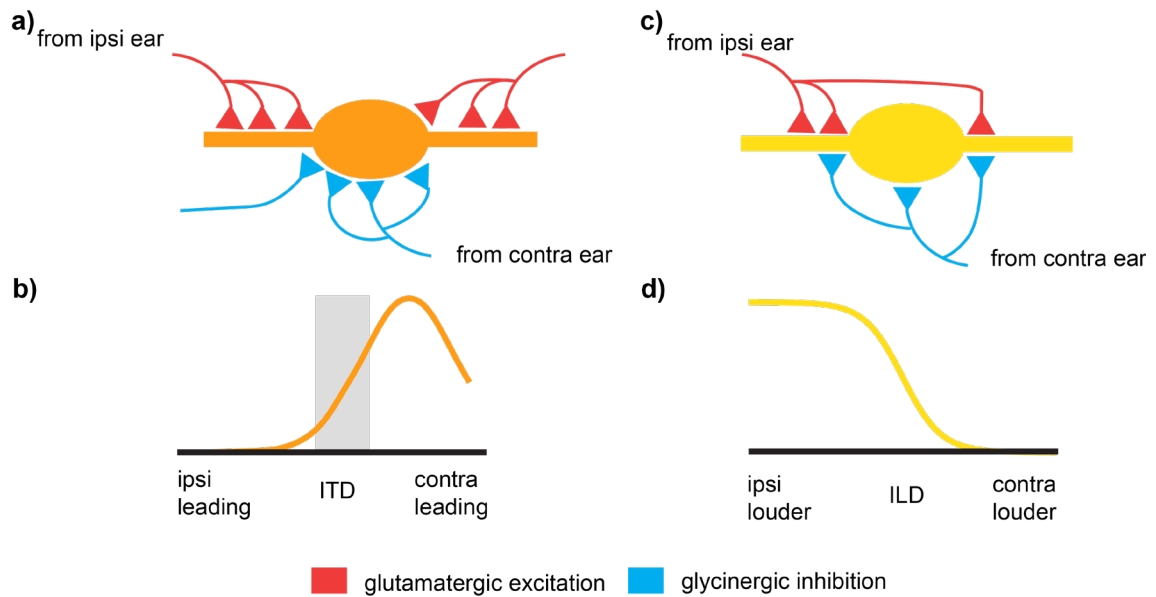
**Figure 3:** The neural basis of ITD and ILD computation in mammals.
(a) A MSO neuron and its synaptic inputs. The MSO is the primary site for ITD computation. Bilateral excitatory (red) and inhibitory (blue) inputs converge on the MSO neuron (orange) being temporally integrated thus enabling ITD sensitivity.
(b) An ITD tuning function of an MSO neuron. ITD tuning functions obtained from MSO neurons commonly peak outside the range of physiologically detectable ITDs (grey area).
(c) A LSO neuron and its synaptic inputs. The LSO is the primary site for ILD computation. Excitatory (red) inputs from the ipsilateral ear and inhibitory (blue) inputs from the contralateral ear converge at the LSO neuron (yellow) creating ILD sensitivity.
(d) An ILD tuning function of an LSO neuron with its characteristic sigmoidal shape. Contralateral ILDs will lead to complete inhibition and ipsilateral ILDs to complete excitation resulting in the sigmoidal shape characteristic for LSO neurons.
With permission after Grothe et al. (2010).

The structure that initially performs ILD detection in mammals is the lateral superior olive (LSO). The LSO is innervated by excitatory inputs from the ipsilateral ear as well as by inhibitory inputs from the contralateral ear (Figure 3c; Grothe et al. 2010). Similar to MSO neurons, LSO neurons display broad ILD tuning functions with a characteristic sigmoidal shape where sounds that are louder at the contralateral ear lead to complete inhibition and *vice versa* (Figure 3d; Grothe et al. 2010). In addition, also the IC, where *de novo* ILD computation occurs as a result of monaural excitation from the cochlear nucleus and binaural inhibition originating from the LSO (Grothe et al. 2010), has been found to exhibit broad ILD tuning (Schnupp and King 1997). Thus, also ILD computation in mammals seems not to depend on a Jeffress-like arrangement.

The sharp tuning curves that are observed for ITDs in the NL of birds are a direct consequence of their function as prime coincidence detectors. In contrast, ITD tuning curves of MSO neurons are found to be broad, eventually peaking outside the physiological range of detectable ITD. Therefore it is assumed that the optimal coding strategy for ITD processing in mammals is the steepest slope where changes in spike rate are greatest (McAlpine et al. 2001; Brand et al. 2002; Pecka et al. 2008). Similar LSO neurons have broad ILD tuning functions with slopes closely centered to frontal positions. Likewise, the LSO has been suggested to employ rate coding (Grothe and Pecka 2014).

## 1.3.    Auditory space representation in mammals

The broad tuning functions observed in ILD and ITD processing have inspired new models of mammalian sound localization favoring hemispheric rate coding over Jeffress-like place coding by means of sharply tuned neurons. Two opponent hemispherical tuned-channels (left and right auditory space) have been proposed to enable sound localization via relative changes in the firing rates of these channels (McAlpine et al. 2001; Phillips and Hall 2005; Stecker et al. 2005; Vigneault-MacLean et al. 2007; Grothe et al. 2010; Briley et al. 2013; Grothe and Pecka 2014).

One consequence of these models is that adaptation to a lateralized sound source should shift the perceived midline of these channels (the intersection of their firing rates) by fatiguing the adapted channel thus biasing perception of subsequent locations. Indeed, human psychophysics has been able to show that spatial judgements depend on prior stimulation (Phillips and Hall 2005; Vigneault-MacLean et al. 2007; Stange et al. 2013).

Similar has been observed on the neural level. Across multiple brain areas of the ascending auditory pathway including the MSO (Stange et al. 2013), LSO (Magnusson et al. 2008; Park et al. 2008), IC (Dahmen et al. 2010) and AC (Lee

and Middlebrooks 2011) the spatial tuning of neurons has been found to depend on the acoustic context.

As a consequence, when probing sound localization performance in humans by presenting a preceding adaptor Lingner et al. (2018) found sound source discrimination to improve close to the adaptor. However, absolute localization accuracy was found to decrease. Improved sound source discrimination in response to a preceding adaptor stimulus has also been observed by Getzmann (2004). Together, these studies suggest that mammalian sound localization is relative rather than absolute, serving the purpose of sound segregation. Here, opponent-coding schemes might constitute efficient means to enable mammals to react with the adequate flexibility to changes in the environment.

However, it is possible that sound localization by means of two channel coding is insufficient. More recently it has been proposed that mammals might use an additional midline channel. Performing psychophysical experiments in humans, Dingle et al. (2010) found subjects to report subsequent test tones closer to the midline despite undergoing symmetrical adaptation before. This is not to be expected in case of two-channel coding as in case of symmetrical adaptation both of the channels should receive equal fatigue not shifting the perceived midline. This therefore argues in favor of a supplemental midline channel. Furthermore, obtaining electroencephalographic recordings from the AC in humans, Briley et al. (2016) reported midline adaption after prior stimulation with a midline adaptor. This complements previous models of two-channel coding as the effect is best explained by the existence of a midline channel. Such an additional channel might potentially serve to make sound localization more robust towards the front.

Focusing on the subcortical structures of the ascending auditory pathway I have reviewed previous work illustrating that mammals do not exploit a

Jeffress-like processing of binaural cues to achieve an absolute representation of auditory space but rather seem to rely on a relative representation by means of rate coding and consequently seem to lack a map of auditory space in all of these structures. However, the long standing, yet erroneous, view that mammals inherited their tympanic ears from birds and the concomitant (implicit) assumption that mammals would exploit a similar neural machinery still has a great impact on research probing the representation of auditory space in the mammalian AC.

## 1.4. The AC is involved in sound localization

Multiple studies have shown that unilateral ablation of the AC results in a deficit to localize sounds in the contralateral hemifield, whereas localization performance in the ipsilateral hemifield usually remains intact (see e.g., Jenkins and Masterton 1982; Jenkins and Merzenich 1984). Bilateral ablating the AC however impairs sound localization abilities across the horizontal plane (see e.g., Heffner and Masterton 1975; Heffner and Heffner 1990). In line with these experiments reversible lesion studies also report deficient localization in the contralateral hemifield following unilateral silencing of the AC and deficient localization across the horizontal plane following bilateral AC silencing (Malhotra et al. 2004; Smith et al. 2004; Malhotra et al. 2008). Together, these studies imply that each AC is involved in the orchestration of sound localization behavior in the opposite hemifield.

## 1.5. The AC and the representation of auditory space

The seminal work by Knudsen and Konishi (1978) and Knudsen (1982) that convincingly showed the presence of an auditory space map in the midbrain structures of the barn owl has inspired decades of electrophysiological experiments in search for a map of auditory space in the AC of mammals, which initially seemed to be a "low-hanging fruit" (Middlebrooks 2021, p. 5772). In a pivotal study Middlebrooks and Pettigrew (1981) aimed to determine such a map

in the AC of anesthetized cats, but to their surprise failed to do so. Instead, they observed that the great majority of neurons recorded exhibited broad contralateral tuning. Subsequent research across different mammalian species fostered this view (Imig et al. 1990; Rajan et al. 1990a; Rajan et al. 1990b; Clarey et al. 1994; Middlebrooks et al. 1998; Mrsic-Flogel et al. 2005; Nelken et al. 2008; Yao et al. 2013; Panniello et al. 2018). Therefore, it has become accepted in auditory neuroscience that the mammalian AC lacks a map of auditory space and represents the contralateral hemifield by means of neurons broadly tuned to the contralateral side.

However, with the gradual shift in auditory neuroscience towards awake preparations a somewhat different, yet inconsistent, picture has emerged, challenging the existing view of rigorous broad contralateral tuning in the AC. Recording from awake cats Mickey and Middlebrooks (2003) observed a slightly more diverse representation of auditory space than reported by previous anesthetized studies – but nevertheless found the great majority of neurons coding best for contralateral positions. Similar observations were made by Woods et al. (2006) when recording from alert macaques. More recent studies in marmoset monkeys (Zhou and Wang 2012; Remington and Wang 2019) have emphasized a more distinct pattern with noteworthy amounts of neurons exhibiting ipsi- or frontal tuning as well. Furthermore, when comparing their results to prior data obtained from anesthetized animals Mickey and Middlebrooks (2003) observed that spatial tuning width of AC neurons was decreased in awake animals. In summary, these reports suggest that spatial tuning of AC neurons in awake animals is different from spatial tuning in anesthetized animals.

### 1.6.  Limitations of previous research studying space representation in the AC

So far research has largely ignored the potential effects of anesthesia on AC's spatial sensitivity. It is known that fewer neurons exhibit frequency tuning under anesthesia (Gaese and Ostwald 2001; Noda and Takahashi 2015) and that frequency tuned neurons respond with fewer spikes to pure tones thus showing an overall decrease in stimulus related activity (Cheung et al. 2001; Gaese and Ostwald 2001; Kato et al. 2015; Noda and Takahashi 2015). It might be possible that similar applies to neurons sensitive for auditory spatial stimulation but this remains to be tested.

Although there has been an increasing number of studies making use of awake preparations, our current knowledge about auditory space coding in the AC still heavily relies on the large pool of data gathered from anesthetized preparations. Despite the emerging picture that the representation of auditory space might be somewhat different in awake animals (see section 1.5), research still is deficient of a direct comparison demonstrating the exact manner in which anesthesia modifies single-cell and population auditory space representation in the AC. Thus, it remains obscure to which degree the rich data pool that has been obtained from anesthetized animals over decades of intense research can be transferred to awake animals.

Indeed, not only under anesthesia might neurons change their spatial tuning. In recent years, there has been a growing body of literature showing that tuning properties of individual neurons change over days and weeks despite a stable population code. This has been observed in various brain regions. For example, Driscoll et al. (2017) performed chronic recordings of posterior parietal cortex (PPC) neurons while mice engaged in a navigation task. Activity patterns of single neurons were found to change but information readout remained stable on the population level. Similar was observed by Aschauer et al. (2019).

Chronically probing the frequency tuning of neurons in the AC of mice the authors observed individual neurons to shift, lose or gain their frequency tuning. However, the population of neurons seemed to maintain an equilibrium of frequency tuning. Similar has been observed in other brain areas including the motor cortex (Rokni et al. 2007; Huber et al. 2012) and the hippocampus (Ziv et al. 2013). However, long-term dynamics in AC single-cell spatial tuning and potential effects upon population coding of auditory space have not been addressed so far.

To date, nearly all studies that investigated space representation in the AC relied upon electrophysiology. While this technique allows for sampling of neurons' spiking activity with extreme high temporal precision, the picture that this method draws is biased. Although new probes allow for the simultaneous recording of hundreds of neurons these measurements are still limited to locations near the electrode. Even more important though is the fact that electrophysiology is prone to oversample highly active neurons. Although this method provides extremely precise insights in the firing behavior of individual neurons, it is practically impossible to obtain a comprehensive picture of the population code when using this technique as is the acquisition of chronic recordings. Therefore, to address questions about the population code and to chronically dissect spatial tuning properties of neurons in the AC, a complementary approach is required.

## 1.7. Two-photon imaging to chronically probe the activity of neural populations

One tool that provides solutions to the aforementioned issues is functional imaging. Since its introduction in 1990 (Denk et al. 1990) two-photon-imaging has emerged as the leading tool for functional imaging. It builds upon the effect of two-photon-absorption first predicted by Göppert-Mayer (1931) and later experimentally observed by Kaiser and Garrett (1961). Two-photon-absorption

describes the simultaneous absorption of two photons of identical frequency to lift a molecule or atom from a low-energy (ground) state into an excited state of higher energy. This effect can be exploited when combined with a fluorescent substance.

Fluorescence is usually achieved by exciting a fluorescent molecule with light of shorter wavelength (higher energy) than will be emitted by the fluorophore following excitation (Stokes shift; Figure 4a). However, if two photons of identical wavelength are simultaneously absorbed by the fluorophore their energies combine. Therefore, double the wavelength (essentially half the energy) can also be used to excite the fluorophore if two-photon absorption is ensured.

However, under normal conditions the probability of two-photon absorption to happen is extremely low (Helmchen and Denk 2005), thus to occur regularly under experimental conditions two-photon absorption is enforced by using femtosecond pulsed lasers that create a peak flux of exciting photons and by confining the laser beam through an objective.

Two-photon microscopy has notable advantages over its one-photon counterpart. For example, only at the objective's focal point will the density of photons be high enough to excite the fluorophore and cause fluorescence, thus restricting photodamage to the focal point (Figure 4b). In addition, because fluorescence is restricted to the focal point any emitted photon collected by the objective must have been emitted by the focal point increasing the signal-to-noise ratio in comparison to one-photon/confocal microscopy. Lastly, the use of longer wavelengths (commonly in the near-infrared range) for two-photon fluorophore excitation allows for deeper tissue penetration (~500-600 µm) which would be impeded when using light of shorter wavelength (commonly more blue-shifted) which is required in conventional one-photon microscopy (max. ~100 µm).
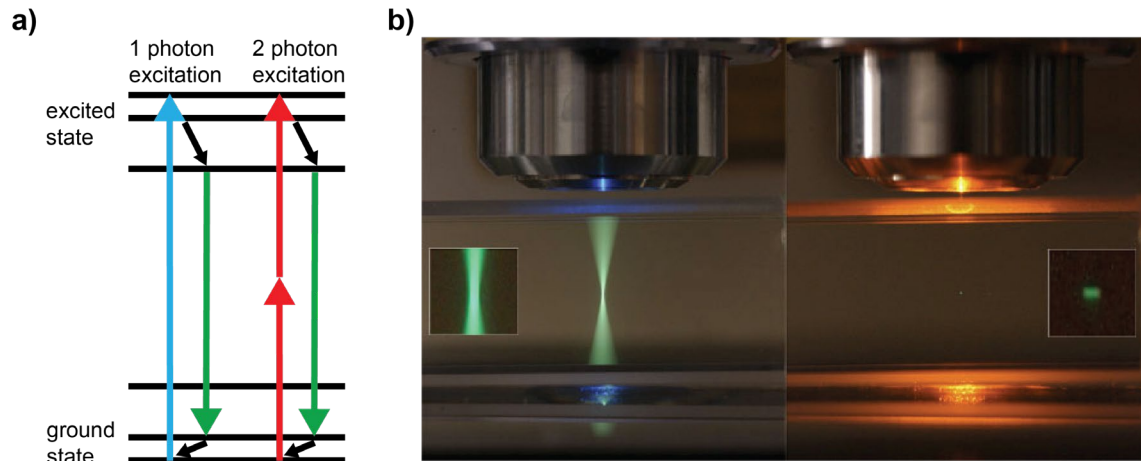
**Figure 4:** Principles of two-photon imaging.
(a) Jablonski diagram illustrating one- and two-photon excitation of a fluorophore. One-photon excitation: Absorption of a single short-wavelength photon of high energy allows for excitation of the fluorophore. Once in its excited state, the fluorophore emits energy by releasing a photon of lower energy (i.e. higher wavelength). Two-photon excitation: The absorption of two photons allows achieving similar as the absorption of a single photon. However, both the photons carry only half the energy required to excite the fluorophore and therefore are of longer wavelength.
(b) Spatial confinement of one- and two-photon absorption. In one-photon imaging the entire cone used to excite the focal plane is excited. In contrast, in two-photon imaging only at the focal point is the density of photons high enough to achieve two-photon absorption thus significantly improving the signal-to-noise ratio. Picture with permission from Steve Ruzin (UC Berkeley).

It was not until the advent of genetically encoded calcium indicators (GECIs) that chronic functional imaging of large neuronal populations by means of two-photon imaging has gained wide application. Calcium indicators translate changes in intracellular calcium concentrations into changes in fluorescence. As neural activity is accompanied by increases in intracellular calcium concentrations, these indicators serve as proxies for the readout of cell activity. GECIs are protein based calcium indicators allowing for virus-based transduction of cells, with GCaMP being the most widely used class of GECIs nowadays. GCaMP combines a derivate of jellyfish derived green fluorescent protein (GFP; Chalfie et al. 1994), with the calcium binding protein calmodulin (CaM) and M13, which is a peptide derived from myosin light chain kinase (Nakai et al. 2001). When lacking calcium the protein fluoresces only weakly. Upon the binding of calcium conformational changes occur, restoring the original structure of the GFP thereby markedly increasing the fluorescence intensity of

the protein. The most sophisticated versions of these proteins nowadays have critically improved sensitivity, temporal resolution and signal-to-noise ratio (Chen et al. 2013). However, even the most advanced GECIs introduce significant delays in reporting cell activity due to their relatively slow kinetics. In addition, the number of action potentials elicited cannot be accurately determined as GECIs behave in a very non-linear fashion. Nevertheless, the combination of GECIs and two-photon imaging has revolutionized neuroscience as it allows to chronically probe the activity of large populations of neurons *in vivo* with unprecedented spatial resolution and simultaneously correlate these activity patterns with the animal's experience (Helmchen and Denk 2005).

## 1.8. The mouse as a model organism to study the neural basis of spatial hearing

To date, most of auditory research on cortical spatial processing has been conducted in cats, albeit other higher mammals such as monkeys and ferrets have been investigated. Only very seldom have studies made use of rodents, such as mice. This might be surprising since mice have by now become the leading animal model in neuroscience given the great abundance of genetic toolboxes available for this species (Ellenbroek and Youn 2016). Furthermore, mice are an especially appealing species for functional imaging by means of two-photon imaging as they are small in brain size which allows for relatively deep tissue penetration and GECIs have successfully been expressed in this species (see e.g. Chen et al. 2013). Although, their acoustic spatial resolution is poorer than for example that of humans (Mills 1958) or cats (Martin and Webster 1987; Huang and May 1996) mice nevertheless can localize sounds with an accuracy of ~30° (Heffner et al. 2001; Lauer et al. 2011; Behrens and Klump 2016). Some mice strains such as the widely used C57BL/6 strain exhibit high frequency hearing loss already after a few weeks of age (Ison et al. 2007). CBA/CaJ mice in contrast are not affected by high frequency hearing loss (Zheng et al. 1999). Therefore,

CBA/CaJ mice are a prime model organism when probing questions about mammalian spatial hearing in combination with two-photon calcium imaging.

### 1.9. Motivation to study the AC and objectives of the PhD thesis

When I started my doctoral project, the features of spatial tuning of neurons in the AC of anesthetized mammals had been characterized in great detail. Still, the precise effects of anesthesia upon the representation of auditory space in the AC have remained elusive. Therefore, I decided to investigate the effects that anesthesia exerts on the spatial sensitivity of the AC as well as its effects on the cortical representation of auditory space. This will be the theme pervasive to this dissertation. In addition, an increasing number of scientific inquiries has recently been concerned with uncovering potential dynamics immanent to neural populations in various brain regions. This has inspired me to do likewise for the representation of space in the AC. Multiple studies – most of which were performed in anesthetized preparations – have revealed a lack of an auditory space map in the AC. To corroborate these reports I also probed the presence or absence of such a map in the AC. By performing chronic two-photon calcium imaging in the AC of awake and anesthetized mice while exposing them to free-field spatial stimulation I set out to tackle these questions.

# 2. MATERIALS AND METHODS

## 2.1. Animals

All animal procedures were approved by the ethical review committee of the local government (*Regierung von Oberbayern;* animal license number: ROB-55.22532.Vet_02-17-221) and carried out in compliance with the German animal welfare laws. Experimental subjects were male CBA/CaJ mice (Jackson Laboratories; Stock No: 000654; age: ~10 weeks; Figure 5a). The mice were kept at a 12/12 hour light/dark cycle and had *ad libitum* access to water and food at all times. A total of eight mice were used in this study. Data was obtained from six animals. Two animals could not be used for imaging due to sprout of a fibrotic-like tissue above the dura mater and were excluded from the experiments (see section 2.2 for more details).

## 2.2. Surgical procedures

Prior to surgery animals were anesthetized with an intraperitoneal injection of a mixture of fentanyl (0.05 mg/kg; Hexal), midazolam (5 mg/kg; Ratiopharm) and medetomidine hydrochloride (0.5 mg/kg; Orion Pharma). Animals also received a subcutaneous injection of the non-steroidal anti-inflammatory drug carprofen (5 mg/kg; Zoetis). Once fully anesthetized, animals were placed on a heating pad to maintain a stable body temperature. The head was fixated using a custom-made stereotactic frame. Following head-fixation, the eyes were covered with eye ointment (Isopto-Max, Alcon Pharma) to prevent corneal drying. The animals' depth of anesthesia was monitored using the toe pinch reflex and observation of the respiratory pattern. The skin of the skull was locally anesthetized using 10% lidocaine (Xylocaine, AstraZeneca). Following one minute of working time, a circular patch of skin was removed (~1 cm$^2$) to expose lambda, bregma and the bone sutures. The periosteum was removed using small dental brushes (Adjustable Precision Applicator Brushes, Parkell) and forceps. The skull was cleaned and the skull surface was then roughened by

application of a dentin activator (Universal Dentin Activator Gel, Parkell) for 10 seconds. The skull was cleaned again with sterile cortex buffer (125 mM NaCl, 5 mM KCl, 10 mM glucose, 10 mM HEPES, 2 mM $CaCl_2 \times 2H_2O$, 2 mM $MgSO_4 \times 7H_2O$) to remove any residual activator. Using a scalpel, the exposed bone was then carefully scratched in a grid-like fashion to facilitate later head bar attachment. The bottom part of the head bar was also roughened to increase adherence to the skull using a dental drill. A thin layer of cyanoacrylate adhesive (Ultra Gel, Pattex) was applied to the bottom of the head bar. Immediately afterwards, the head bar was positioned on top of the skull along the median longitudinal fissure. The superglue hardened for two minutes before dental cement (C&B Metabond, Parkell) was applied to increase the bonding of head bar and skull. The mouse was then relocated to another custom-made stereotactic frame, where the head bar could be fixated. After skin removal, lidocaine was applied to the left temporal muscle, and the muscle was removed after an appropriate waiting time for the local anesthetic to operate. A small craniotomy was made using a 3 mm handheld biopsy punch to expose the target brain area with the dura left intact. The location of the AC was estimated using vascular landmarks (Joachimsthaler et al. 2014). These landmarks were also used to determine the location of the injection sites.

Adeno-associated virus (AAV) encoding the GECI GCaMP6s and mRuby2 as a structural marker under the control of the synapsin 1 promoter using (AAV2/1.Syn.mRuby2.GSG.P2A.GCaMP6s.WPRE.SV40, Penn Vector Core) was then injected into the brain using pipettes of pulled glass capillaries (puller: P-97, Sutter Instruments; glass capillaries: 408472, Hilgenberg GmbH with tip diameter 40-50 µm). At four sites (spaced ~500 µm apart), pipettes were slowly moved to ~350 µm deep below the pial surface using a hydraulic micromanipulator (HO-10, Narishige). The tissue was then given one minute to recover before the virus injection was started. About 250 nl of the viral construct diluted (1:1) with sterile

cortex buffer was pressure injected into the selected target area using a micro-injection system adjusted to ~20 psi, ejecting ~10 nl/min, delivered every 5 s with an opening time of 20 ms (Picospritzer III, Toohey). To prevent virus from leakage the tissue was given one minute recovery time before the glass pipette was removed in steps of 100 µm and a waiting period of one minute between the steps. Upon skull opening great care was taken that the brain was kept moist in cortex buffer throughout the entire injection procedure. Following the injections, an Ø 3 mm circular glass coverslip (No. 1, Ref 41001103, Glasswarenfabrik Karl Hecht) was used to cover the craniotomy. The window was then sealed with cyanoacrylate adhesive. Both the head bar and cover glass were then further stabilized using dental cement (Paladur, Heraeus Kulzer). Any loose skin was then fixated with tissue glue (Histoacryl, B. Braun).

At the end of the surgical procedure general anesthesia was reversed with an intraperitoneal injection of Naloxon (1.2 mg/kg; Ratiopharm), Flumazenil (0.5 mg/kg; Hexal) and Atipamezole (2.5 mg/kg; Orion Pharma). Carprofen was administered 24h and 48h after surgery. Animals were kept for about two hours under a heat lamp before being transferred to the animal room. The recovery of the animal was monitored for three consecutive days following the surgery, then at the sixth postoperative day and then weekly. Thereafter, beginning with the start of the habituation phase, animal wellbeing was monitored daily until the end of the experiment, when animals were euthanized by means of cervical dislocation.

Prior experience in the laboratory has shown that a few weeks after the initial surgery a certain amount of experimental animals (up to 60 %) tend to suffer from bone regrowth under the craniotomy or the development of a fibrotic-like tissue above the dura mater, thus impeding imaging and necessitating a revision surgery. The fibrotic-like tissue is typically not pervaded by small blood vessels and thus appears to be completely white. If a revision surgery became

necessary, the animal was anesthetized and prepared for surgical procedure as described above. The dental cement and the cyanoacrylate adhesive around the cranial window were then carefully removed using a dental drill (Presto II, NSK; drill bits: HM1 005, Meisinger). Upon excavation, the coverslip was removed, and the brain was exposed. If the animal suffered from bone regrowth, the newly formed bone was carefully removed using forceps and a dental drill. The brain was frequently washed with sterile cortex buffer to ensure moistening of the brain and to wash off any potential bone splinters created by drilling. Afterwards, the dura was carefully peeled off. If the animal suffered from tissue regrowth, the tissue and dura were carefully removed and the brain surface was cleaned with sterile cortex buffer. Then, a new cranial window was inserted, sealed and fixated as described above. Revision surgeries became necessary in two out of eight animals, but were not successful in any of the cases.

## 2.3. Habituation

Two weeks after the surgery, mice were habituated to head-fixation and the experimental setup (Figure 5a/b). Habituation was performed over one week. On the first and second day, animals were accustomed to the experimenter's hand. After starting to crawl on the experimenter's hand, the animal was taken to the setup and given a couple of minutes to explore. On the third day all animals crawled deliberately on the experimenter's hand. Thus, all animals got to explore the setup latest on the third day of handling and got used to ambient noises created by the microscope. On day four, animals were habituated to head fixation. Once head-fixed, animals spent two minutes in the setup. On day five head fixation time was increased to five minutes. On day six and seven, animals were head-fixed for ten minutes while sounds (see section 2.4) were presented occasionally to accustom the animals to stimulus presentation. After every day of habituation the animals received water-soaked food pellets as a reward.

### 2.4. Sounds

All stimuli were presented free field at a sampling rate of 192 kHz in a custom-made sound attenuated chamber at 75 dB SPL. Five small dynamic loudspeakers (model: CDMG15008-03A, CUI Devices) were positioned on a horizontal hoop (5 cm in radius) in 30° increments of azimuth sampling 120° of auditory space (ipsilateral to contralateral speaker positions: +30°, 0°, -30°, -60°, -90°; Figure 5b). Sampling of auditory space was limited to 120° because AC imaging required lateral rotation of the microscope thus preventing sampling of 180° of auditory space (see section 2.5 and Figure 5b). The angular distance between speakers was chosen since the spatial resolution of mice is supposed to be around 30° (Lauer et al. 2011; Behrens and Klump 2016; Heffner et al. 2001).The transfer function of every speaker was measured using a ¼-inch probe microphone (transducer type 4393 and preamplifier type 2670, Brüel&Kjaer, Bremen, Germany) and compensated by filtering the sound files with the inverse transfer function to obtain a flat frequency response between 3 – 70 kHz.

The acoustic stimuli were 10x20 ms noise bursts, delivered at 10 Hz and smoothened with 5 ms cosine onset-offset ramps to avoid edge artifacts. Two categories of sounds were used: white noise and 10 – 20 kHz band-passed noise. The frequency range of the band-passed noise was chosen because mice show their best hearing threshold in this frequency range (Heffner and Masterton 1980; Radziwon et al. 2009).

The sounds were presented pseudorandomly. At each speaker location, each stimulus category was presented 50 times. Therefore, 5x2x50 stimuli were presented in total. The intertrial interval was set to four seconds to account for the decay times of the calcium indicator (Chen et al. 2013). Hence, the entire stimulus protocol took about 33 minutes.

## 2.5.    Chronic in-vivo two-photon imaging
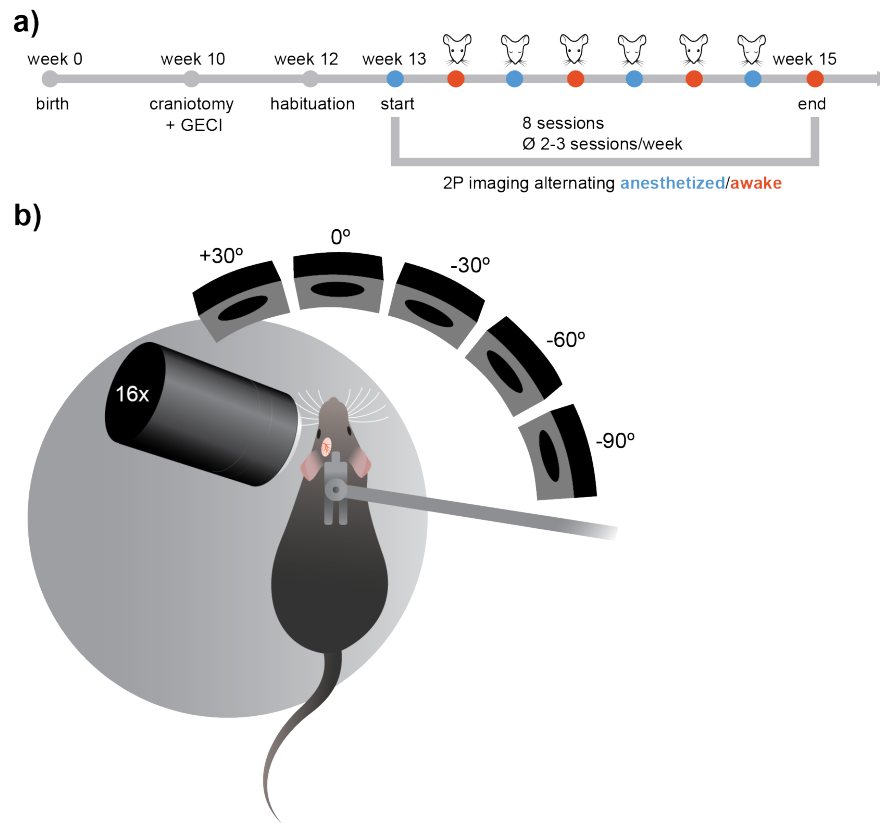


**Figure 5:** Schemata of experimental timeline and setup.
(a) The experimental timeline.
(b) Sketch of the experimental setup. The animal was placed on a running disk with the microscope being tilted by about ~60° to allow imaging of neurons in layer 2/3 of the left AC. For naturalistic auditory spatial stimulation sounds were presented from a free-field speaker array. The array consisted of five speakers each spaced 30°, thus sampling 120° of auditory space.

Three weeks after virus injection, the initial imaging session was performed. In total eight imaging sessions per animal were conducted. At each imaging session, the animal was either anesthetized or awake. The state of the animal was alternated at each imaging session so that in four of the eight imaging sessions the animal was awake (Figure 5a). In the first imaging session, animals were always anesthetized. This allowed easy acquisition of an overview image (size: 1500 x 1500 µm) as well as a reference image (size: 500 x 500 µm), which

served as a ground truth for plane and cell re-finding for the next imaging sessions (Figure 6).
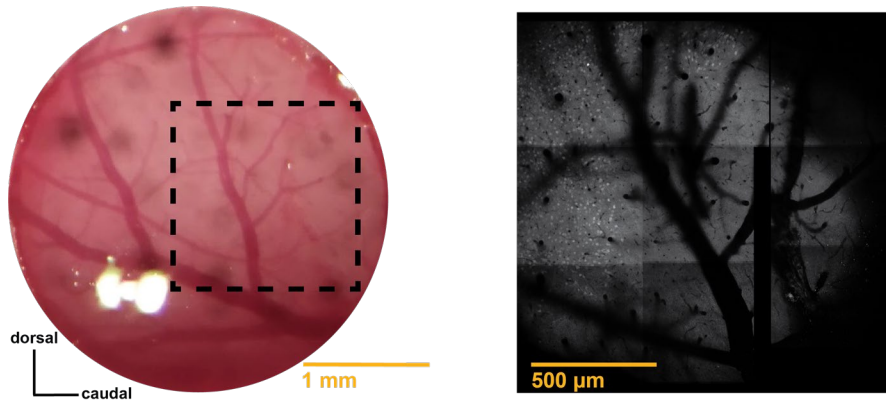


**Figure 6:** Picture of cortical surface and overview image.
The picture on the left shows the cortical surface of an example animal after craniotomy was performed. The black rectangle indicates the position of the overview image (picture on the right) which was acquired as a wide-field image for this animal at the start of the first imaging session.

In all anesthetized imaging sessions, anesthesia was induced with 5% isoflurane at a flow rate of 2.0 l/min for two minutes followed by constant application of 1% isoflurane at a flow rate of 0.75 l/min to maintain anesthesia. A constant body temperature of the animal was ensured through a heating lamp, and the eyes were covered with eye ointment to prevent corneal drying. Animals were placed on an aluminum running disk covered with a silicone mat while being head-fixed. In the awake imaging sessions, animals were allowed to run on the disk at all times. Motor activity (Schneider and Mooney 2018; Musall et al. 2019) as well as shifts in arousal (Lin et al. 2019) have been shown to influence auditory cortical activity. Inspection of a random selection of experiments showed that animals remained mostly still (~90% of recording time). I therefore refrained from treating trials of movements separately. Since animals remained mostly still, shifts in arousal were probably also negligible as arousal has been shown to synchronize with locomotion (McGinley et al. 2015).

Imaging was performed using a 16X, 0.8 NA water immersion objective (Nikon, Tokio, Kantō, Japan) on a Bergamo 2 Series two-photon microscope

(Thorlabs, Newton, NJ, USA) equipped with an 8 kHz resonant scanner driven by a MaiTai eHP DS tunable Ti:Sapphire laser (Spectra Physics, Santa Clara, CA, USA). The GCaMP6s/mRuby2 double construct was excited at 940 nm wavelength at a laser power of 25 – 45 mW. Scans from upper cortical layers 2/3 (imaging depth: ~200 µm below pial surface) of 512 x 512 pixels were acquired at ~30 Hz with a scan zoom factor to achieve an imaging area of 250 x 250 µm (Figure 7).
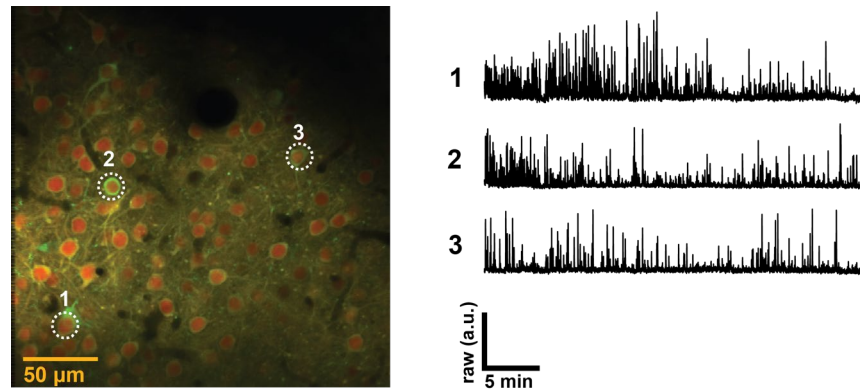


**Figure 7:** Picture of an imaging field and raw calcium transients.
The picture on the left shows an imaging field which was excited at 940 nm at a depth of ~200 µm below the pial surface. The right one shows the raw calcium transients of three exemplary neurons recorded during the imaging session (~33 min) of this imaging field. The locations of these neurons in the imaging field are indicated by the white circles.

To access the AC, which is located on the lateral side of the animal's brain, the microscope had to be rotated by ~60° until the objective was positioned orthogonal to the cranial window. ScanImage software (Pologruto et al. 2003) was used to control the microscope.
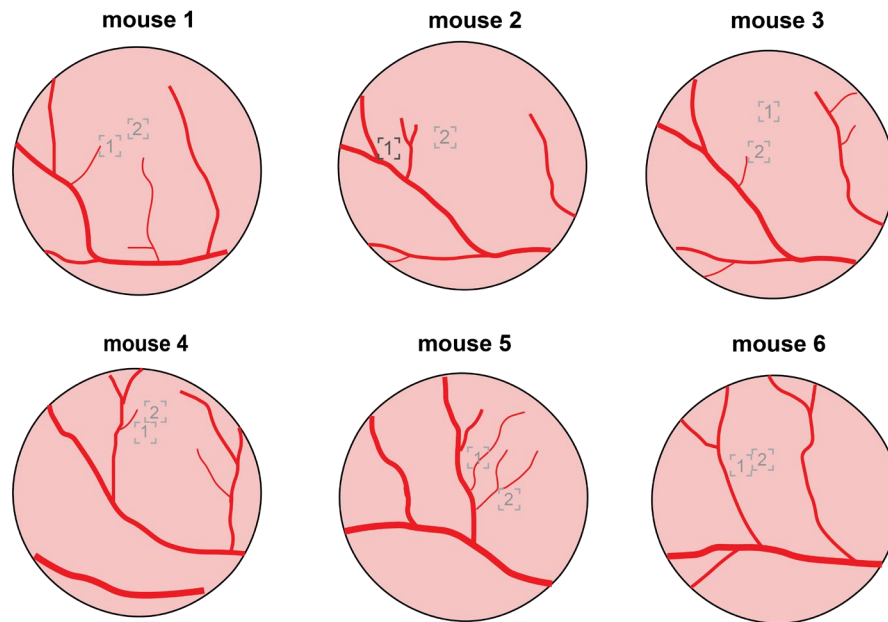
**Figure 8:** Overview of blood vessel patterns and imaging locations.
Shown are the individual blood vessel patterns of each animal and the imaging locations (grey rectangles) associated with each animal. Location 1 of mouse 2 (black rectangle) was excluded from analysis (see section 3). The diameter of the craniotomy was 3 mm whereas each imaging location measured 250 x 250 µm in size.

Two imaging fields were identified per animal based on virus transduction and blood vessel pattern (Figure 8). To ensure imaging of healthy auditory cortical neurons, the imaging fields were finally selected based on detection of spontaneous activity as well as sound-evoked responses of neurons. For each imaging field, the stimulus protocol was run. Thus, imaging took on average about 1.25 h per animal, including cell re-finding. After each imaging session, the animal was given 1-2 days to recover before the next imaging session was performed. Thus, all eight imaging sessions were conducted over a time course of about three weeks.

## 2.6. Data analysis

Data analysis was performed using custom-written MATLAB (Mathworks) routines.

### 2.6.1. Data preprocessing

First, images were corrected for movement artifacts using a discrete Fourier transform algorithm. Individual trials were excluded from further analysis if motion was greater than 10 pixels. Afterwards, sequences of every 5 frames were averaged to obtain a final frame rate of about 6 Hz. After each imaging session, a time-averaged image was generated from all recorded frames for each imaging location. For each location one of these time-averaged images was selected to serve as a reference location and thus allowed for re-finding of cells in the remaining recordings. Then, using a semi-automatic approach regions of interest (ROIs) were identified in the reference image. In a first step a custom-written algorithm was used to detect cell bodies based on pixel-wise correlations in the activity channel as well as the average image derived from the structural marker. In a second step, the quality of automatic ROI identification was manually controlled. Wherever the automatic detection approach proved inaccurate, ROIs were manually added, removed or readjusted. In a next step, the identified ROIs were automatically matched to the remaining experiments. Again, this step was manually controlled, and ROIs were readjusted if necessary. If ROIs could not be re-found in a certain experiment, these ROIs were excluded from the analysis for that particular experiment.

The use of a functional calcium indicator in combination with a structural marker allowed for ratiometric imaging. For each ROI, the fluorescence signal of each channel at each time frame was calculated as the average fluorescence of all pixels inside the ROI. A neuropil correction was performed to each ROI's activity fluorescence time series using a contamination ratio of r = 0.7. The green and red fluorescent signals were calculated as follows:

$$F_{green\ ROI}(t) = F_{green\ measured}(t) - r \times F_{green\ neuropil}(t)$$

$$F_{red\ ROI}(t) = F_{red\ measured}(t)$$

The ratio was then calculated as:

$$R(t) = \frac{F_{green\,ROI}\,(t)}{F_{red\,ROI}\,(t)}$$

The baseline corrected ratio was then calculated as:

$$\frac{\Delta R}{R_0} = \frac{R - R_0}{R_0} - 1$$

The baseline $R_0$ was the mean baseline ratio signal of each trial obtained over a one second period prior to stimulus onset, and the activity window R was the second following stimulus onset.

For each ROI, the response strength to sound stimulation was calculated. Therefore, the change in fluorescence was compared across two time windows. The baseline period that comprised the time prior to stimulus onset (-1 – 0 sec relative to stimulus onset) and the response time window which comprised the time after stimulus onset (0 – 1 sec relative to stimulus onset). For each ROI the trial average response strength was then calculated as the maximum change in fluorescence during the response time window relative to the baseline average.

Single trials were rejected based on the following criteria: 1) the mean baseline fluorescence was higher than 110% of the average of all baselines for that particular session, which indicates preceding activity and therefore unreliable transient detection; 2) the standard deviation of the baseline was higher than 0.1 normalized ΔR/R units, which indicates that the baseline was unstable or particularly noisy.

To assess the spatial sensitivity of ROIs in each imaging session, the responses to the different speaker positions were compared. Depending on the sample size a one-way ANOVA (alpha = 0.05; ≥ 25 samples per speaker position) or a Kruskal-Wallis (alpha = 0.05; < 25 samples per speaker position) was performed to detect statistically significant differences. Post-hoc multiple

comparisons (alpha = 0.05) were performed to determine between which speaker positions the responses proved statistically different. In case of statistical significance in the ANOVA or in the Kruskal-Wallis test and in the multiple comparisons, the ROI was defined to be spatially modulated (Figure 9).
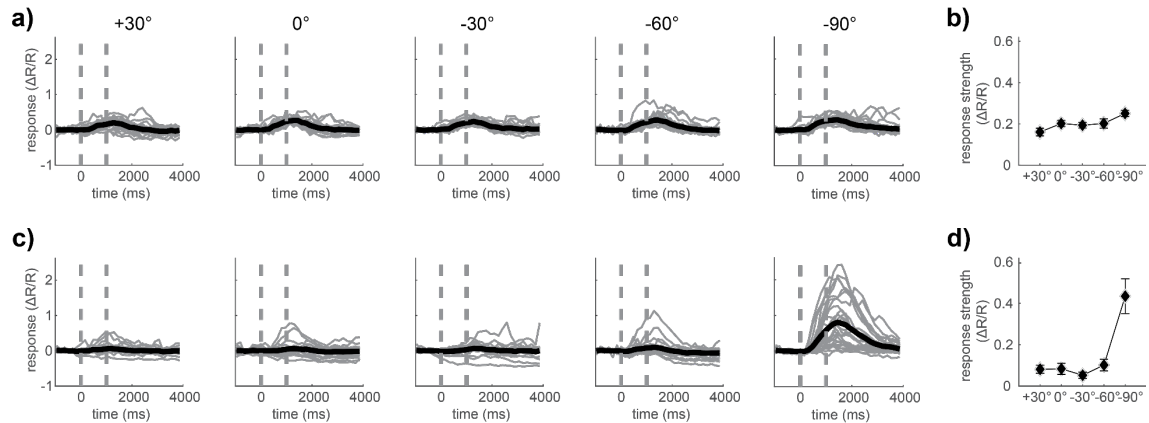


**Figure 9:** Example traces of two neurons.
(a) Shown are the responses of a neuron that was not spatially modulated when presented with band-passed noise bursts from different speaker positions. Grey traces indicate individual responses. The black lines show the average responses to each speaker locations. Dashed grey lines show the time of stimulus on- and offset.
(b) Average response amplitudes of the neuron shown in (a) to the various speaker locations. Error bars denote the standard error of the mean.
(c) and (d) Same as in (a) and (b) but for a neuron that was spatially modulated when presented with band-passed noise bursts from different speaker positions.

For each spatially modulated ROI the best speaker position was determined as the speaker location eliciting the maximum average response strength. Furthermore, the best stimulus category (i.e. white noise or band-passed noise) was determined for each spatially modulated ROI as either the stimulus category under which the ROI was found to be spatially modulated or – in case the ROI was spatially modulated under both categories – the stimulus category eliciting the greater response strength at its respective best speaker position.

### 2.6.2. Analysis of anesthetics effects on the auditory space representation in the AC

To assess potential effects of anesthesia on the cortical representation of auditory space, the calcium responses of ROIs to auditory spatial stimulation from the first anesthetized and the first awake imaging session were compared. A one-sided Wilcoxon rank-sum test was conducted to test if the average response strength of spatially modulated ROIs was greater in the awake than in the anesthetized condition. The same test was applied to see if the tuning width of spatially modulated ROIs was smaller in the awake than in the anesthetized condition (see below for tuning width calculation). A one-sided Wilcoxon rank-sum test was also used to assess if the distribution of the best speaker positions proved to be less contralateral in the awake condition.

For ROIs that were spatially modulated under both conditions, a one-sided Wilcoxon signed-rank test was additionally performed to test if the best speaker position was less contralateral in the awake condition. Furthermore, a one-sided Wilcoxon signed-rank test was run to test if the tuning width of ROIs that were spatially modulated under both conditions was smaller in the awake condition.

The tuning width of a spatially modulated ROI was determined as the distance in both directions from the best speaker position where the cumulative summed response strength was still ≥ 50% of the total response amplitude.

$X^2$ tests were run to test 1) if the number of spatially modulated ROIs differed between the awake and anesthetized condition, 2) if the distributions of best speaker positions were different between the two conditions (for this purpose, the three contralateral speaker positions were pooled together and the ipsilateral and frontal speaker positions were pooled together) and 3) to test if there was a difference in the distribution of tuning curve categories of spatially

modulated ROIs between the awake and anesthetized condition (see below for definition of categories).

To probe the presence or absence of an auditory space map the best speaker positions of the spatially modulated cells were correlated along the optimal direction in dorsoventral-rostrocaudal space for each animal and each condition. The optimal direction was the one in which Pearson's correlation coefficient between best speaker position and tissue coordinate along this direction was maximal. To assess the statistical significance of this correlation a bootstrapping approach was used. The best speaker positions were shuffled along the dorsoventral-rostrocaudal coordinates of the spatially modulated cells and then correlated along the optimal direction. This was performed 10,000 times and yielded the bootstrapped estimate of correlation coefficients. An alpha of 0.05 was adopted and thus if the actual correlation coefficient was $\geq$ to the 95th percentile of the bootstrapped values this indicated a significant correlation of best speaker positions along the optimal direction.

Visual inspection of individual tuning curves of ROIs revealed the existence of four categories of ROIs (Figure 13a). A custom-written classification algorithm was thus used to assign every spatially modulated ROI to one of the following categories based on its tuning curve shape: 1) specifically-tuned: one single speaker won all multiple comparisons; 2) broadly tuned: the only additional speakers that won the multiple comparisons where neighboring speakers; 3) bilobed tuned: two maximal responding speaker positions that were separated by a minimal responding speaker position (in this case, one of the maximal speaker positions had to be significantly different based on the multiple comparisons, whereas the other speaker position had to show a response strength that was at least 150% greater than the detected minimal response) and 4) other: a spatially modulated ROI that could not be assigned to one of the above mentioned categories;

### 2.6.3. Analysis of dynamics in the auditory space representation of the AC

To test for changes in the cortical representation of auditory space over time, the calcium responses of ROIs across the different sessions were compared within the anesthetized as well as within the awake condition. For this, depending on the sample size a two-way ANOVA (alpha = 0.05; factors: session number and speaker position; ≥ 25 samples per speaker position) or a Friedman-test (alpha = 0.05; factors: session number and speaker position; < 25 samples per speaker position) was performed for each ROI that was spatially modulated at least once within a wakefulness condition to test if the spatial response profile of a ROI changed across the sessions.

$X^2$ tests were conducted to test 1) if the number of spatially modulated ROIs that changed their spatial response profile across the various sessions differed between the awake and anesthetized condition and 2) to probe if the number of spatially modulated ROIs differed in each anesthetized imaging session from the number of spatially modulated ROIs in its corresponding awake imaging session and 3) to see if the distribution of the best speaker positions changed across the various sessions within a condition (for this purpose contralateral speaker positions were pooled together and the ipsilateral and frontal speaker positions were pooled together).

One-sided Wilcoxon rank-sum tests were run to determine if in each anesthetized imaging session the average response strength of spatially modulated ROIs was smaller than in the corresponding awake imaging session.

One-sided paired t-tests were run to determine if in each anesthetized imaging session the average stimulus-induced response strength of all ROIs was smaller than in the corresponding awake imaging session.

A one-sided Wilcoxon signed-rank test was performed to test if the distribution of the best speaker positions in awake animals was more

contralateral in the first imaging session compared to the remaining three imaging sessions, i.e. it was used to test if the population of ROIs that were spatially modulated in the first imaging session shifted their best speaker position towards less contralateral positions in subsequent sessions.

# 3. RESULTS

In total I performed imaging in 12 imaging fields with an area of 250 x 250 µm across 6 mice expressing GCamP6s/mRuby2 via injected AAV into the left AC (see section 2). Chronic two-photon calcium imaging was performed over a time course of approximately three weeks. In total, each animal underwent 8 imaging sessions with the state of the animal alternating between anesthetized and awake while being exposed to pulsed band-passed or white noise presented from five different speaker locations (Figure 5b). Post-hoc one imaging field of one animal had to be excluded (mouse 2, location 1; Figure 8). In the first two imaging sessions of this region no spatially modulated cells were detected and further control analyses failed to identify any sound responsive neurons for these two sessions (paired t-tests run separately for each ROI in each session of the imaging field). Post-hoc visual inspection of the topographical position of the imaging field in relation to the blood vessel pattern revealed that the location was outside of AC. Therefore, the calcium transients from 1224 neurons obtained from the remaining 11 imaging fields across the 6 mice were analyzed.

### 3.1.1. Cross-sectional analysis

Based on published (see section 1.6) observations, I wanted to first investigate effects of anesthesia. Namely, I wanted to determine 1) if responses to noise bursts are reduced under anesthesia and 2) if fewer neurons exhibit spatial sensitivity under anesthesia. In addition, I wanted to see if the application of anesthesia changes the neural representation of auditory space in the AC. To date, this issue has not been addressed by means of a direct comparison. To rule out any potentially cumulative effects of anesthesia, the calcium responses of only those neurons that were successfully imaged in the first awake imaging session as well as in the first anesthetized imaging session were compared for this part of the analysis. From the 1224 neurons that were identified based on the reference images 260 neurons (21%) could not be identified in the first

anesthetized or awake imaging session which permitted analysis of the calcium transients obtained from 964 cells.

### 3.1.2. Neural sensitivity in the AC is modified by anesthesia

First, I probed a potential reduction of neural responses under anesthesia when stimulated with noise bursts. Indeed, the average response strength of spatially modulated cells was found to be higher in the awake condition (mean: 0.183 ΔR/R; SEM: 0.020 ΔR/R) than in the anesthetized condition (mean: 0.099 ΔR/R; SEM: 0.003 ΔR/R; Figure 10a). This difference was statistically significant (one-sided Wilcoxon rank-sum test; $p < 0.001$; $z = 8.074$) indicating that responses to noise bursts in the AC are diminished under anesthesia.
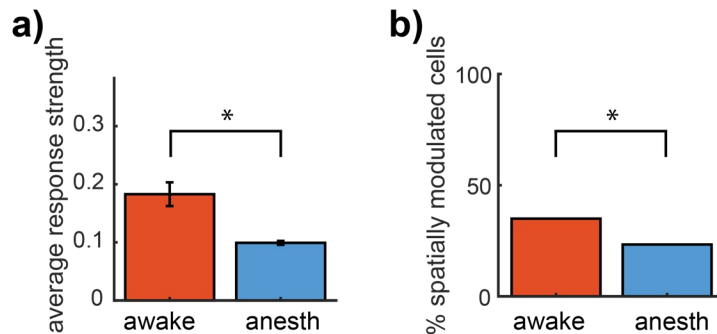


**Figure 10**: Neural sensitivity is decreased under anesthesia.
(a) Average stimulus-related response strength of spatially modulated neurons when animals were awake (red bar) and anesthetized (blue bar).
(b) Percentage of neurons that are spatially modulated in the awake (red bar) and anesthetized (blue bar) condition.

Next, I investigated if the spatial sensitivity of neurons was altered by anesthesia. In the awake condition I observed that a higher number of neurons was spatially modulated (n = 337 neurons / 34.97%) than in the anesthetized condition (n = 225 / 23.34%) as was confirmed by statistics ($p < 0.001$; $X^2 = 31.503$; Figure 10b). Thus, fewer neurons in the AC show spatial sensitivity under anesthesia.

### 3.1.3. Anesthesia modifies the representation of auditory space in the AC

By imaging from the same neurons under both conditions, effects of anesthesia on single-cell and population responses in the AC to spatial

stimulation were investigated. My analysis revealed that across all spatially modulated neurons the best speaker positions were differently distributed in anesthetized and awake animals (awake ipsi to contra = 31 : 76 : 47 : 54 : 129; anesthetized ipsi to contra = 13 : 6 : 10 : 104 : 92; $p < 0.001$; $X^2 = 42.135$; Figure 11a). Visual inspection of these distributions indicated that in the awake state the population of spatially modulated cells appeared to prefer less contralateral best speaker positions than that recorded in the anesthetized state. This was confirmed by statistics (one-sided Wilcoxon rank-sum test; $p < 0.001$; $z = -4.386$). I found neurons that were spatially modulated exclusively in the awake (n = 244 / 25.31%) or in the anesthetized (n = 132 / 13.69%) condition but also neurons that were spatially modulated under both conditions (n = 93 / 9.65%). The neurons that were spatially modulated in both conditions appeared to shift their best speaker positions towards less contralateral positions in the awake session (Figure 11b). This was confirmed by statistics (one-sided Wilcoxon signed-rank test; $p = 0.001$; $z = 2.993$). Taken together, these results clearly show that in awake animals the population response is less lateralized than in anesthetized animals and so is the spatial preference of single neurons spatially modulated under both conditions.
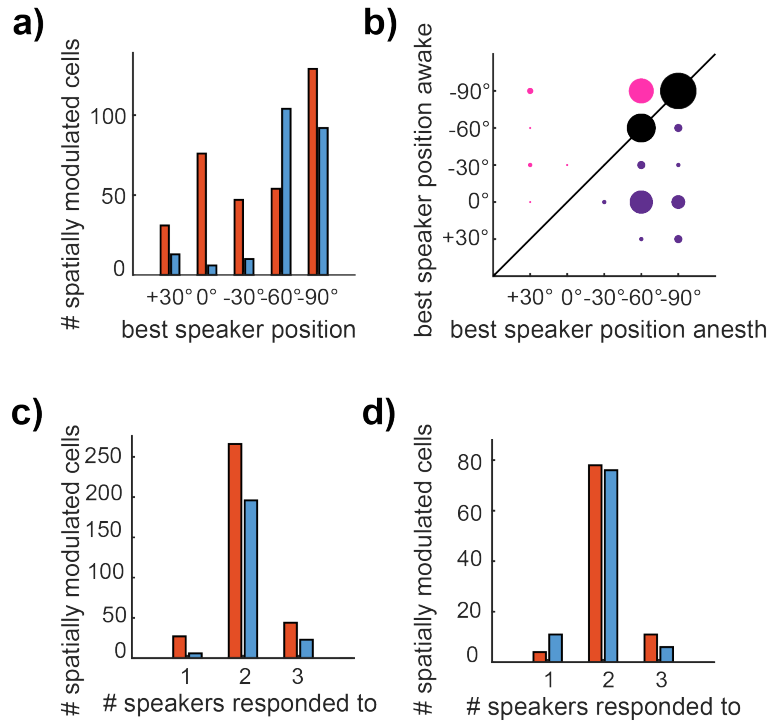
**Figure 11:** Comparison of spatial tuning properties in awake and anesthetized animals based on best speaker and tuning width distribution.

(a) Distribution of the best speaker position for spatially modulated cells in awake (red bars) and anesthetized (blue bars) animals.

(b) Comparison of the best speaker position of neurons that were spatially modulated in the awake as well as in the anesthetized condition. The black line indicates the line of unity. The circle size indicates the number of neurons with greater circle size representing more spatially modulated neurons. Black circles show neurons that did not shift their best speaker position between the conditions. Magenta circles indicate neurons that shifted their best speaker position towards more contralateral speaker positions in the awake condition. Purple circles indicate neurons that shifted their best speaker position towards less contralateral positions in the awake condition.

(c) Distributions of tuning width for all spatially modulated neurons in awake (red bars) and anesthetized (blue bars) animals.

(d) Same as (c) but for the cells that were spatially modulated in the anesthetized as well as in the awake condition.

Since I observed that anesthesia altered the population response of spatially modulated neurons as well as the best speaker position of single neurons, I was intrigued to find out if anesthesia modified the tuning width of neurons as well. Following a prior report by Mickey and Middlebrooks (2003) (see section 1.5), I specifically tested if the tuning width of spatially modulated neurons was decreased in awake animals. There was no evidence that tuning width was smaller in awake animals neither for the whole population of spatially

modulated neurons (one-sided Wilcoxon rank-sum test; p = 0.269, z = -0.616; Figure 11c) nor for the subpopulation of neurons that was spatially modulated under both conditions (one-sided Wilcoxon signed-rank test; p = 0.984, z = 2.139; Figure 11d).

In summary, these results show that auditory space is differently represented in the AC in awake animals. In the awake animal more neurons prefer central speaker positions than in the anesthetized state (Figure 11a/b). Importantly, this disparity in preferential spatial tuning – both on the population as well as on the single-cell level – cannot be explained by an increase in tuning width (Figure 11c/d).

### 3.1.4. Absence of an auditory space map in the AC

**a)**
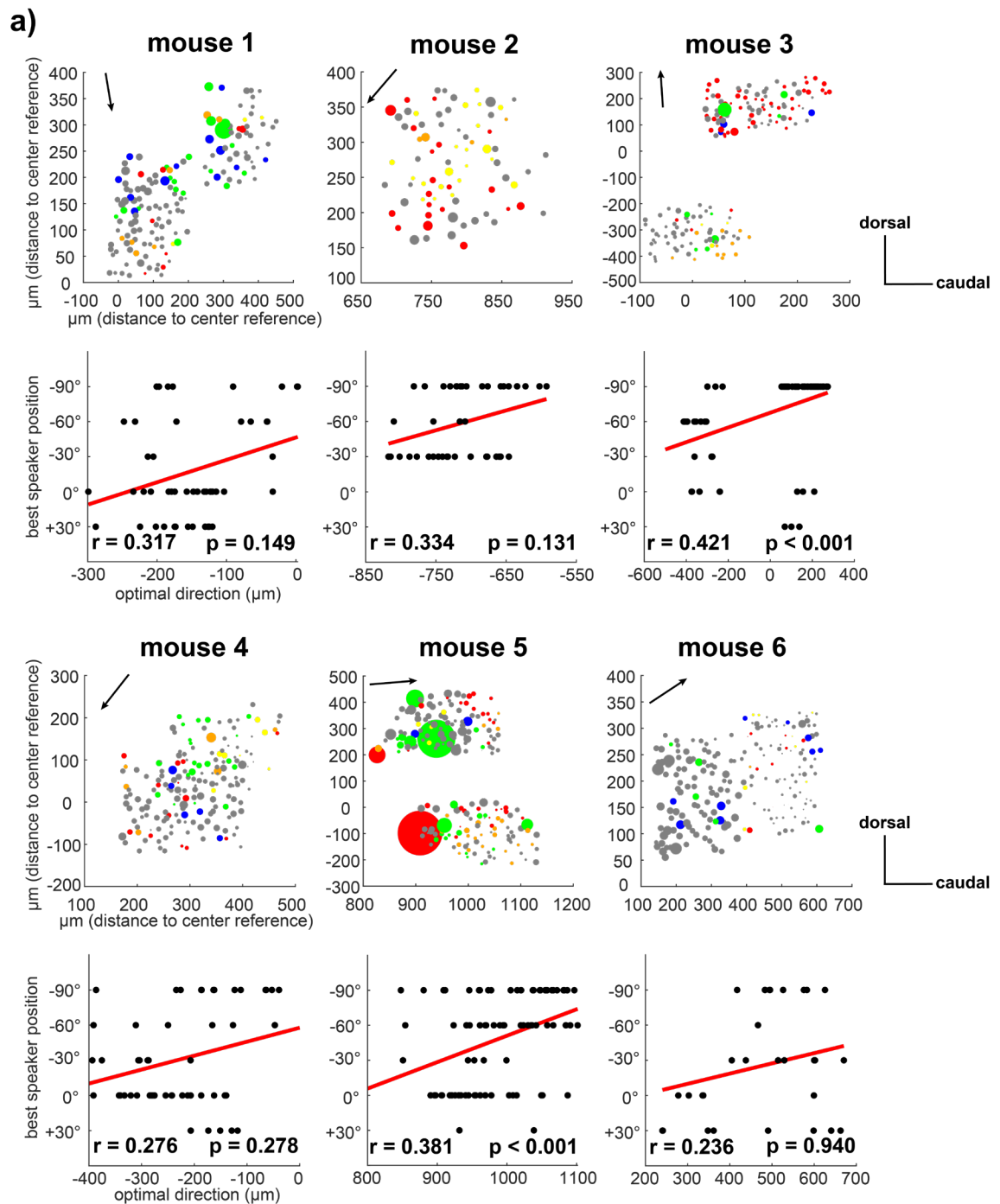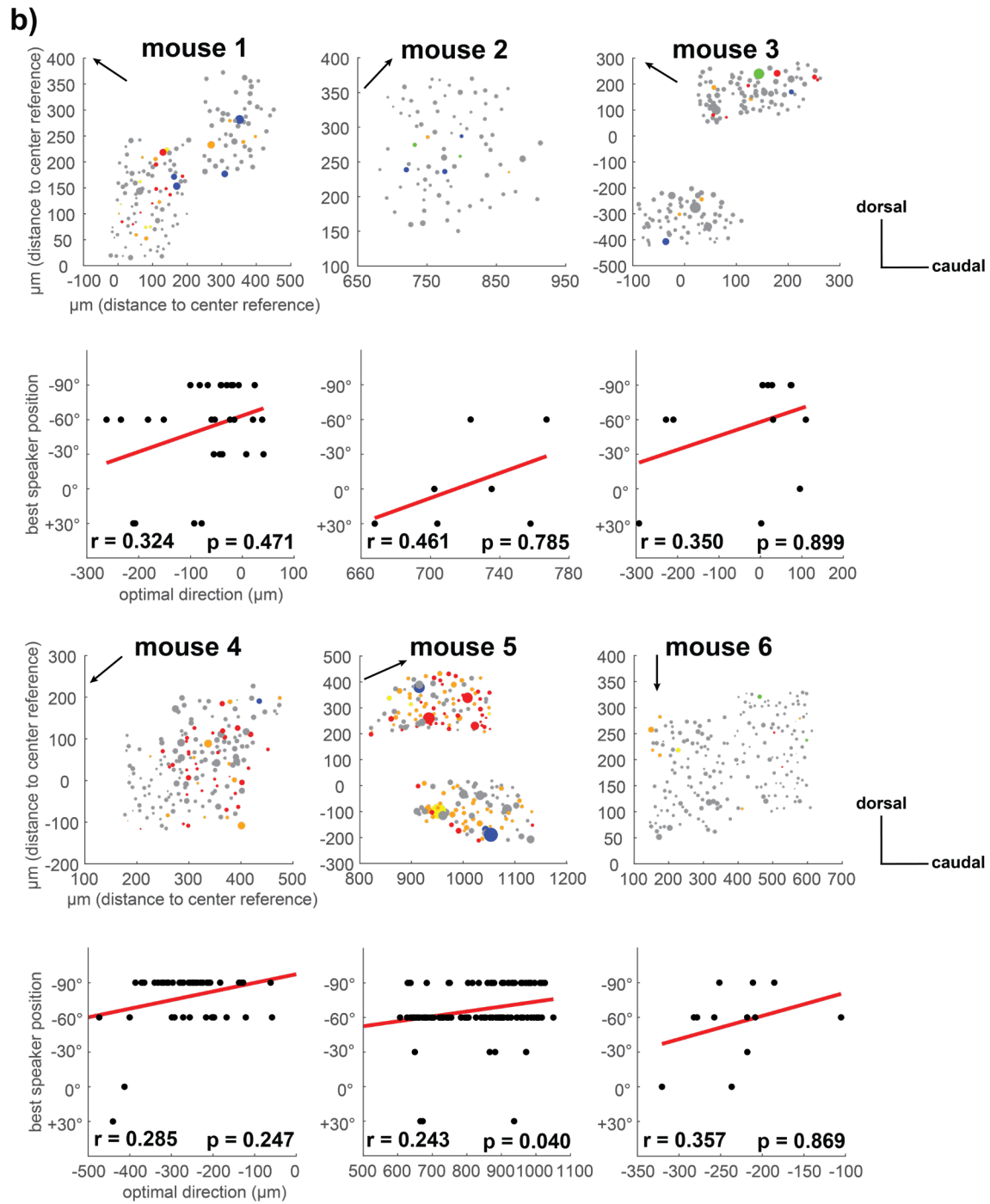
**Figure 12:** The AC lacks a topographical map of auditory space.
(a) Top row: Topographical layout of imaged neurons with respect to their reference image in awake animals. Neurons are color coded by their best speaker position. Size of each neuron indicates the average response strength of that neuron. Blue = +30°, green = 0°, yellow = -30°, orange = -60°, red = -90°, grey = not spatially modulated. Bottom row: Correlations of best speaker positions along the optimal direction in dorsoventral-rostrocaudal space in awake animals. The optimal direction of each correlation is shown by the arrow in the topographical layout for each animal.
(b) Same as (a) but for anesthetized animals.

To probe the presence or absence of an auditory space map in the AC of anesthetized and awake mice, I correlated the best speaker positions of the spatially modulated cells along the optimal direction in dorsoventral-rostrocaudal space separately for each mouse and each condition (see section 2.6.2; Figure 12). In most animals correlations of best speaker positions along the optimal direction were not significant (mouse 1 awake: $r = 0.317$, $p = 0.149$; mouse 2 awake: $r = 0.334$, $p = 0.131$; mouse 3 awake: $r = 0.421$, $p < 0.001$; mouse 4 awake: $r = 0.276$, $p = 0.278$; mouse 5 awake: $r = 0.381$, $p < 0.001$; mouse 6 awake: $r = 0.236$, $p = 0.940$; mouse 1 anesthetized: $r = 0.324$, $p = 0.471$; mouse 2 anesthetized: $r = 0.461$, $p = 0.785$; mouse 3 anesthetized: $r = 0.350$, $p = 0.899$; mouse 4 anesthetized: $r = 0.285$, $p = 0.247$; mouse 5 anesthetized: $r = 0.243$, $p = 0.040$; mouse 6 anesthetized: $r = 0.357$, $p = 0.869$). For the few mice in which significant correlation coefficients were detected (mouse 3 awake; mouse 5 awake & anesthetized) correlation coefficients were mild ($r < 0.5$) indicative of only a weak structure of best speaker positions across the cortical surface in these animals. Indeed, visual inspection of the topographical layout of the respective mice supports this notion. The correlations in these animals seemed to be caused by local clusters of neurons preferring similar best speaker positions. However, even within these clusters neurons responding best to distant speaker positions could be observed. In sum, despite local clusters of similar tuned neurons were detectable in some animals, true maps of auditory space were absent in both anesthetized and awake animals.

### 3.1.5. Categorization of shapes of spatial tuning curves in the AC

Based on tuning curves as they have been shown and reported in previous studies (Middlebrooks and Pettigrew 1981; Imig et al. 1990; Rajan et al. 1990a; Middlebrooks et al. 1998; Mickey and Middlebrooks 2003; Irvine et al. 1996; Mrsic-Flogel et al. 2005) and visual inspection of neural tuning curves from calcium responses obtained in the present dataset, it seemed reasonable to

assume that spatially modulated neurons commonly fall into one of three categories based on the shape of their tuning curves: specifically-tuned neurons, broadly-tuned neurons and bilobed-tuned neurons (Figure 13a). Specifically-tuned neurons were defined as neurons with sharp spatial tuning by responding to only one single speaker position, whereas neurons that responded to two or more neighboring speaker positions were classified as broadly-tuned neurons. In contrast, neurons that had two non-neighboring maxima separated by a through and thus exhibited more complex tuning curves were defined as bilobed-tuned neurons.
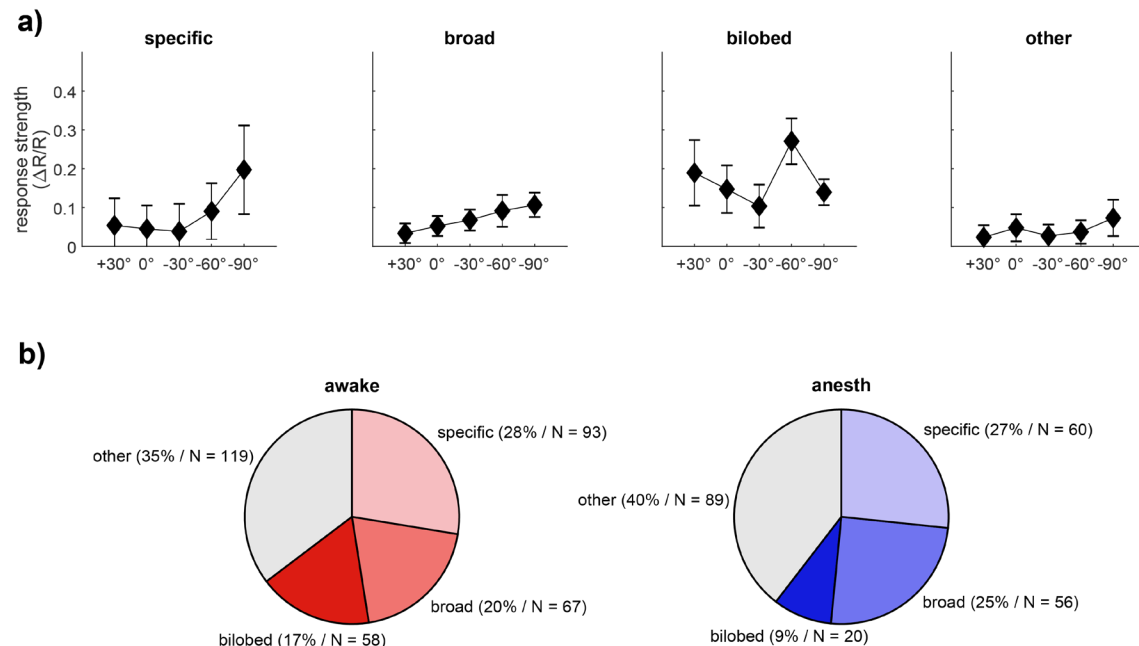


**Figure 13**: Classification of shapes of neuronal tuning curves.
(a) Shown are the tuning curves of four spatially modulated neurons. Each neuron belongs to a different class based on the shape of its tuning curve. In total, three classes were determined (*specific*, *broad* and *bilobed*). In addition, a fourth class (*other*) was introduced to capture also neurons that did not fall into any of the three prior categories. Tuning curves show the average responses to the various speaker positions with error bars denoting the standard error of the mean.
(b) Overview of the distribution of the shapes of spatial tuning curves for spatially modulated neurons in awake (left pie chart) and anesthetized (right pie chart) animals.

In order to characterize and categorize the shapes of tuning curves of spatially modulated neurons in an unbiased manner, I performed an automatic classification of these tuning curves (see section 2.6.2). This classification of

tuning curves (Figure 13a) revealed that in the awake animal the majority of classified neurons were specifically-tuned neurons (n = 93, 28%), followed by broadly-tuned neurons (n = 67, 20%) and bilobed-tuned neurons (n = 58, 17%). Thirty five percent of neurons (n = 119) could not be attributed to any of the categories and were therefore identified as *other*. In the anesthetized animal the distribution revealed a somewhat distinct pattern. Most neurons were identified as specifically-tuned neurons (n = 60, 27%). Fewer neurons were categorized as broadly-tuned neurons (n = 56, 25%) and bilobed-tuned neurons (n = 20, 9%). Again, the majority of neurons was not assigned to any of the classes and was therefore referred to as *other* (n = 89, 40%). Statistics revealed that the distributions of categories did differ between anesthetized and awake animals (p = 0.030; $X^2$ = 5.616). This difference stems from the increase of bilobed-tuned neurons in awake animals and a decrease in broadly-tuned neurons (Figure 13b). Thus, spatial tuning seems to be more complex in awake animals than in anesthetized animals.

## 3.2.    Longitudinal analysis

To probe the long-term stability of spatially tuned neurons, I extended the cross-sectional approach and performed chronic imaging of the same neurons over multiple days under awake and anesthetized conditions. This allowed me to assess the dynamics of the cortical representation of auditory space and any potential cumulative effects of anesthesia on AC neurons. Of the 1224 neurons that were identified in the reference experiments 573 neurons (46%) could not be successfully identified in the remaining experiments and had to be excluded from further analysis. Thus, for this part of the analysis the calcium transients from 651 neurons were examined.

### 3.2.1.  Dynamics of neural sensitivity in the AC

By taking stimulus induced response strength as well as the number of spatially modulated neurons as proxies for sound-evoked neural sensitivity, my

previous results revealed that sound-evoked neural sensitivity in the AC is decreased under anesthesia (see section 3.1.2). To assess if the decrease in neural sensitivity that I observed persists over time, I first looked at the stimulus-induced response strength of neurons across sessions in both conditions. Throughout all imaging sessions the average stimulus-induced response strength of neurons was smaller in anesthetized animals. This effect was observed for the spatially modulated cells ($n_{awake}$ = 429; mean ± SEM: 0.117 ± 0.005 ΔR/R (awake session 1); 0.078 ± 0.004 ΔR/R (awake session 2); 0.068 ± 0.003 ΔR/R (awake session 3); 0.065 ± 0.003 ΔR/R (awake session 4) / $n_{anesthetized}$ = 222; 0.102 ± 0.009 ΔR/R (anesthetized session 1); 0.062 ± 0.008 ΔR/R (anesthetized session 2); 0.056 ± 0.005 ΔR/R (anesthetized session 3); 0.051 ± 0.005 ΔR/R (anesthetized session 4); Figure 14a) and confirmed by statistics (one-sided Wilcoxon rank-sum test; awake session 1 vs anesthetized session 1: $p < 0.001$, $z = 4.353$; awake session 2 vs anesthetized session 2: $p < 0.001$, $z = 6.814$; awake session 3 vs anesthetized session 3: $p= 0.008$, $z = 2.408$; awake session 4 vs anesthetized session 4: $p < 0.001$, $z = 5.672$). Also for the whole population of neurons imaged throughout the average stimulus-induced response strength was smaller in anesthetized animals ($n = 651$; mean ± SEM: 0.086 ± 0.0004 (awake session 1); 0.054 ± 0.0003 ΔR/R (awake session 2); 0.048 ± 0.0003 ΔR/R (awake session 3); 0.046 ± 0.0003 ΔR/R (awake session 4) / 0.059 ± 0.0003 ΔR/R (anesthetized session 1); 0.024 ± 0.0002 ΔR/R (anesthetized session 2); 0.028 ± 0.0002 ΔR/R (anesthetized session 3); 0.034 ± 0.0002 ΔR/R (anesthetized session 4); Figure 14b). These differences were statistically significant (one-sided paired t-test; awake session 1 vs anesthetized session 1: $p < 0.001$, $t = 7.332$; awake session 2 vs anesthetized session 2: $p < 0.001$, $t = 9.150$; awake session 3 vs anesthetized session 3: $p < 0.001$, $t = 7.747$; awake session 4 vs anesthetized session 4: $p < 0.001$, $t = 5.928$). This permanent decreased stimulus-induced response strength of neurons under anesthesia suggests that neural sensitivity is consistently diminished when animals are exposed to anesthesia.
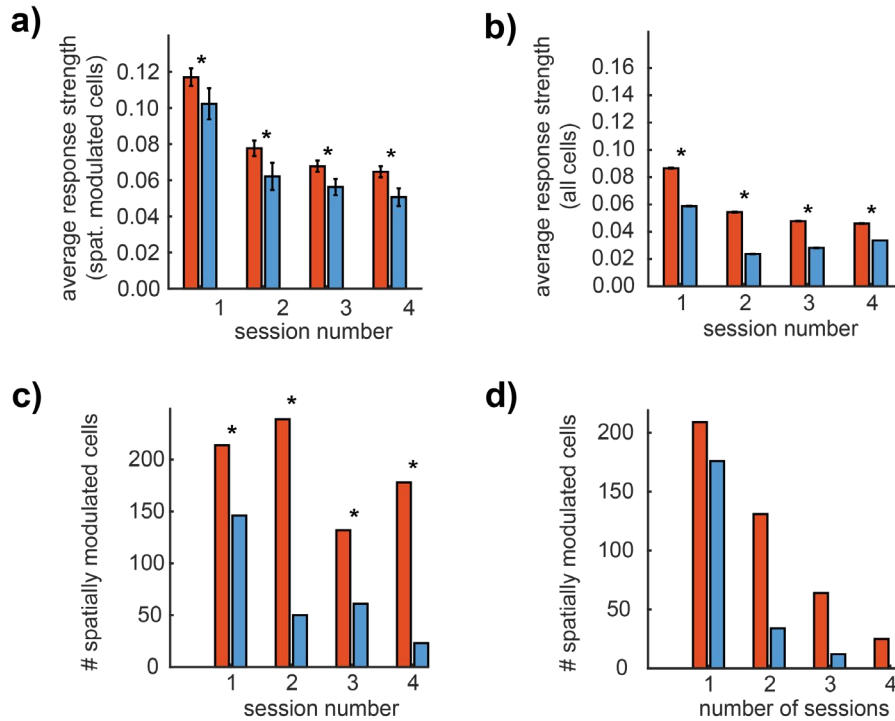
**Figure 14:** Neural sensitivity is chronically decreased under anesthesia.
(a) Average stimulus-related response strength of all spatially modulated cells across imaging sessions for awake (red bar) and anesthetized (blue bar) animals. Error bars denote the standard error of the mean.
(b) Same as (a) but for the average stimulus-related response strength of all cells across imaging sessions.
(c) Number of neurons for awake (red bars) and anesthetized (blue bars) animals that were spatially modulated in each session.
(d) Number of spatially modulated neurons in awake (red bars) and anesthetized animals (blue bars) shown for the number of sessions in which they were spatially modulated.

Plotting the number of neurons that were spatially modulated in each session (Figure 14c) revealed that across all sessions more neurons were spatially modulated if the animals were awake (awake session 1 : anesthetized session 1 = 214 : 146; awake session 2 : anesthetized session 2 = 239 : 50; awake session 3 : anesthetized session 3 = 132 : 61; awake session 4 : anesthetized session 4 = 178 : 23). These differences were statistically significant (session 1: $p < 0.001$, $X^2 =$ 17.753; session 2: $p < 0.001$, $X^2 = 158.865$; session 3: $p < 0.001$, $X^2 = 29.935$; session 4: $p < 0.001$, $X^2 = 141.348$). This is in line with my "snapshot" observation made in section 3.1.2 that fewer neurons are spatially modulated if animals are anesthetized. In summary, I observed that response strength as well as the

number of spatially sensitive neurons was constantly decreased under anesthesia, indicating that anesthesia consistently reduces the sound-evoked sensitivity of neurons.

I was also interested to see if spatially modulated neurons would remain responsive over time. When plotting the number of spatially modulated neurons against the number of sessions in which they were found to be spatially modulated (Figure 14d) it became apparent that most of the cells were spatially modulated in one out of four sessions only. In the awake animal 209 out of 409 cells (51.10%) were spatially modulated in one single session only. 131 (32.03%) neurons were spatially modulated in two sessions, 64 (15.89%) were identified to be spatially modulated in three sessions and only 25 (6.11%) neurons were found to be spatially modulated in all four sessions. A similar trend could be observed for the anesthetized animal. Out of 222 cells 176 (79.28%) were spatially modulated in one single session only 34 (15.32%) cells were spatially modulated in two sessions. In three sessions 12 (5.41%) cells were spatially modulated. No cell was found to be spatially modulated in all four sessions when anesthetized. In conclusion, the great majority of neurons lost or gained their spatial sensitivity over time. This effect was observed in awake as well as anesthetized animals

Chronic exposure to imaging can result in rundown effects of neuronal response strength (internal communication within the lab). Repeated imaging might eventually lead to a cumulative reduction of neural sensitivity and thus challenge the results presented here. A reduction in neural response strength might manifest in a continuous decrement of stimulus-induced response but also could reflect in a systematic decrease in the number of spatially modulated cells. Plotting average stimulus-induced response strength against the session number revealed that only between the first and second session a decline in the response strength is apparent but then seems to settle in an equilibrium. This effect could be observed for all the neurons (mean ± SEM: $0.086 \pm 0.0004$ $\Delta R/R$ (awake session 1); $0.054 \pm 0.0003$ $\Delta R/R$ (awake session 2); $0.048 \pm 0.0003$ $\Delta R/R$ (awake session 3);

0.046 ± 0.0003 ΔR/R (awake session 4) / 0.059 ± 0.0003 ΔR/R (anesthetized session 1); 0.024 ± 0.0002 ΔR/R (anesthetized session 2); 0.028 ± 0.0002 ΔR/R (anesthetized session 3); 0.034 ± 0.0002 ΔR/R (anesthetized session 4); Figure 14b). The same applied to the spatially modulated cells only (mean ± SEM: 0.117 ± 0.005 ΔR/R (awake session 1); 0.078 ± 0.004 ΔR/R (awake session 2); 0.068 ± 0.003 ΔR/R (awake session 3); 0.065 ± 0.003 ΔR/R (awake session 4) / 0.102 ± 0.009 ΔR/R (anesthetized session 1); 0.062 ± 0.008 ΔR/R (anesthetized session 2); 0.056 ± 0.005 ΔR/R (anesthetized session 3); 0.051 ± 0.005 ΔR/R (anesthetized session 4); Figure 14a). This trend was independent of the alertness state of the animals. Furthermore, plotting the number of spatially modulated cells across the session number of imaging sessions revealed that in fact in the anesthetized animal the number of spatially modulated cells decreased over time (session 1 : session 2 : session 3 : session 4 = 146 cells : 50 cells : 61 cells : 23 cells), however this effect was not observed when animals were awake (session 1 : session 2 : session 3 : session 4 = 214 cells : 239 cells : 132 cells : 178 cells; Figure 14c). Visual inspection of tuning curves of individual cells assured that the decrease in spatial sensitivity in anesthetized animals was in fact a loss of spatial sensitivity and not a non-observance of spatial sensitivity by statistics due to a decrease in response strength. Thus, in sum, except for the first two sessions no relevant decrease in sound-evoked response strength could be observed – independent of the alertness state of the animal. Furthermore, the number of spatially modulated cells only lessened in the anesthetized condition. Therefore, taken together, chronic exposure to imaging did not to affect sound-evoked neural sensitivity in a cumulative manner.

### 3.2.2. Dynamics in the cortical representation of auditory space in the AC

Next, I tracked the same neurons over multiple days and investigated if their tuning curves varied over time. Statistics revealed that in both conditions more than 80% of spatially modulated cells showed a shift in their spatial tuning

curve across sessions (awake: 83.68%; anesthetized: 83.78%; Figure 15a). There was no difference in the amount of spatially modulated neurons changing their tuning curves over time between anesthetized and awake animals (p = 0.249; $X^2$ = 1.329). These results show that on a single-cell level spatial tuning is highly dynamic and that these dynamics are independent of the state of the animal.
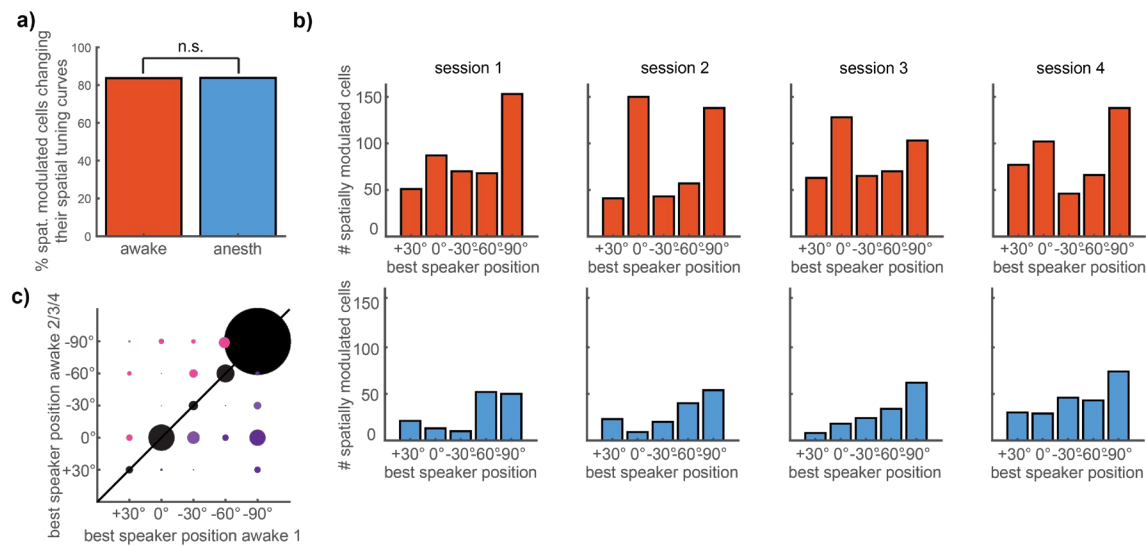


**Figure 15**: Long-term dynamics in the cortical representation of auditory space.
(a) Percentage of neurons for awake (red bar) and anesthetized (blue bar) animals that showed a shift in their spatial tuning curve over imaging sessions.
(b) Distribution of the best speaker positions for spatially-modulated cells in awake (red bars) and anesthetized (blue bars) animals across imaging sessions.
(c) Comparison of the best speaker positions of neurons that remained spatially modulated over all awake imaging sessions. The black line indicates the line of unity. The circle size indicates the number of neurons, with greater circle size representing more spatially modulated neurons. Black circles show neurons that did not shift their best speaker position over sessions. Magenta circles indicate neurons that shifted their best speaker position towards more contralateral speaker positions over time. Purple circles indicate neurons that shifted their best speaker position towards less contralateral positions over time.

Despite the strong dynamics in single-cell spatial tuning a stable representation of auditory space might be achieved by reliable population responses. Therefore, by pooling the three contralateral speaker positions together and the ipsilateral and frontal speaker positions together, I compared the distributions of the best speaker positions across the various imaging sessions for each condition.

I first compared the distributions from the awake sessions. Between the first and second session the distribution of the best speaker positions changed (p < 0.001; $X^2$ = 13.848) but then remained stable (session 2 versus session 3: p = 1.000; $X^2$ = 0.000; session 3 versus session 4: p = 0.408; $X^2$ = 0.684; Figure 15b top row). In line with this observation, I saw a shift towards less contralateral speaker positions over time, when comparing the best speaker positions of neurons in the first session against the remaining sessions (Figure 15c) for neurons that were spatially modulated in the remaining sessions with respect to the first session (n = 224). Analysis revealed that this shift was statistically significant (one-sided Wilcoxon signed-rank test; p = 0.011; z = 2.277). Taken together, in awake animals, following an initial shift towards a less contralateral representation the population settles in an equilibrium. Thus, despite high variability in single-cell spatial tuning the neural population maintains stable thus likely enabling a stable representation of auditory space.

Next, I repeated the comparison for the anesthetized sessions. I observed, that throughout all sessions the distributions of best speaker position did not differ (session 1 versus session 2: p = 0.780, $X^2$ = 0.078; session 2 versus session 3: p = 0.380, $X^2$ = 0.775; session 3 versus session 4: p = 0.051, $X^2$ = 3.812; Figure 15b bottom row). Similar to the population in awake animals, the population of spatially modulated cells in anesthetized animals maintained an equilibrium of best speaker position distributions. However, the initial shift seen in awake animals was absent in the anesthetized preparation, indicating that under anesthesia the population of neurons was more stable than when awake.

In summary, repeated imaging of the same population of neurons in awake and anesthetized animals confirmed and extended the results obtained from the cross-sectional approach. Overall, I observed that across all imaging sessions sound-induced response strength (Figure 14a/b) as well as the spatial sensitivity of neurons (Figure 14d) was smaller under anesthesia. Importantly,

there was no sign that repeated exposure did exert cumulative effects on neural sensitivity. Chronic imaging revealed that the majority of neurons lost or gained their spatial sensitivity over time (Figure 14c). Interestingly, single-cell spatial tuning was highly dynamic (Figure 15a), whereas the population of neurons was found to maintain an equilibrium that was more stable in the anesthetized (Figure 15b bottom row) than in the awake animal (Figure 15b top row; Figure 15c). Therefore, while spatial coding in the AC is highly dynamic on the single-cell level, the population code remains stable over time, despite repeated exposure to anesthesia.

# 4. DISCUSSION

## 4.1. Overview of results

Performing chronic two-photon calcium imaging of neurons in the AC of awake and anesthetized mice, I investigated the effects of anesthesia on the representation of auditory space and probed the stability of spatial representation over days and weeks. Under anesthesia sound-evoked responses were attenuated and fewer neurons exhibited spatial tuning. Notably, anesthesia suppressed the representation of frontal locations both on the single-cell and the population level. The width of spatial tuning, in contrast, was not affected by anesthesia but the shapes of tuning functions were more complex when animals were awake. In both awake and anesthetized animals, the AC was lacking a topographic map of auditory space. Long-term imaging of neurons showed that single-cell spatial tuning was extremely noisy and dynamic. The majority of neurons lost or gained their spatial sensitivity over days and weeks and most of those neurons also changed their spatial tuning curves over this time course. Thus different neurons with ever-changing spatial tuning contributed to the population response on different days. Despite this drift on the single-cell level the population response maintained an equilibrium, e.g. assuring a markedly stable representation of frontal locations in awake animals.

In the following paragraphs I will discuss the functions and mechanisms which could underlie my observations. I will also elaborate on the limitations of my study. Finally, I will end by outlining possible directions for future research and concluding remarks.

### 4.2. Anesthesia impairs auditory space encoding in the AC

Imaging the identical population of neurons in anesthetized and awake animals I observed reduced sound-evoked responses under anesthesia (Figure 10a). These responses were consistently attenuated under anesthesia (Figure 14a/b). Additionally, more neurons were spatially selective when animals were awake than when animals were anesthetized (Figure 10b; again, this effect persevered across imaging sessions; Figure 14c) demonstrating that AC's susceptibility to spatial stimulation is corrupted by anesthesia. It is tempting to speculate that the observed reduction in stimulus-evoked response strength and the decrease in the number of spatially selective neurons might lead to a deterioration in the encoding of auditory space. Previous research found that neurons in the AC can signal the location of a sound throughout 360° by means of spike count and first spike latency (known as the panoramic code for sound localization; Middlebrooks et al. 1994; Brugge et al. 1996; Eggermont 1998; Middlebrooks et al. 1998; Furukawa and Middlebrooks 2002). When probing AC neurons with pure tones under anesthesia, both parameters have been shown to be affected. Response latency increases under anesthesia (Noda and Takahashi 2015) and the number of spikes elicited is decreased (Gaese and Ostwald 2001; Noda and Takahashi 2015). It is likely that in the present experiment anesthesia changed responses in a similar manner. Although the calcium indicator does not allow for tracking of individual spikes, the magnitude of stimulus-evoked calcium activity can serve as a proxy for the number of spikes elicited. As the activity to noise bursts was reduced under anesthesia, I assume that fewer spikes were elicited. This will inevitably detract AC of an important means to compute

the spatial position of an object. Given the results of prior research, first spike latency was most likely also increased under anesthesia. Such an increase would disrupt sound source localization even more. Since also fewer neurons proved to be spatially sensitive (see above), the AC is additionally left with fewer units collecting information about the encompassing auditory space. For all these reasons, it is conceivable that auditory space encoding is impaired by anesthesia.

## 4.3.    Anesthesia suppresses the representation of frontal positions in the AC

It has become widely accepted in auditory neuroscience that neurons within the mammalian AC are tuned to the contralateral hemifield. However, this view has primarily emerged from studies that were carried out in anesthetized animals (Middlebrooks and Pettigrew 1981; Imig et al. 1990; Rajan et al. 1990a; Rajan et al. 1990b; Clarey et al. 1994; Middlebrooks et al. 1998; Mrsic-Flogel et al. 2005; Yao et al. 2013; Panniello et al. 2018). More recent electrophysiological research performed in awake animals has suggested that the representation of auditory space might underlie a more distributed code but otherwise yielded somewhat incoherent results. Whereas Mickey and Middlebrooks (2003) and Woods et al. (2006) in line with prior anesthetized experiments reported the majority of neurons preferring contralateral stimulus positions, the study performed by Zhou and Wang (2012) and recently by Remington and Wang (2019) highlighted that spatial selectivity might be less lateralized in awake animals. Imaging the identical population of neurons in anesthetized and awake animals I could confirm that the population of neurons indeed prefers more central positions when animals are awake (Figure 11a). However, since no study to date was able to record from the identical group of neurons in anesthetized and awake animals, research has remained ignorant of the specific anesthetic effects on auditory space representation on the single-cell level. I could show that individual cells that were spatially modulated in anesthetized as well as in awake animals, showed a preponderance in awake

animals to shift their best speaker position towards frontal positions (Figure 11b). Hence, anesthesia suppresses the suppression of frontal positions in the AC.

How can this suppression of frontal positions by anesthesia be explained? In mammals ILD computation – the main binaural spatial cue exploited by mice – has been shown to be the result of an exquisitely balanced interplay of excitation (glutamate) and inhibition (glycine) (Grothe et al. 2010). As anesthetics have been shown to enhance inhibition and reduce excitation (see e.g., Ries and Puil 1999; Grasshoff and Antkowiak 2006) it might be tempting to speculate that alterations to this equilibrium by anesthesia cause a bias in ILD computation and thus ultimately create different neural representations of auditory space in awake and anesthetized animals. However, in awake (e.g., Park et al. 2004) as well as in anesthetized animals (e.g., Tollin and Yin 2002) neurons in the LSO, the neural hub of mammalian ILD computation, exhibit broad sigmoidal ILD tuning functions with a preference for ipsilateral positions. This ipsilateral preference is flipped to a contralateral preference higher up in the auditory pathway as LSO neurons target the contralateral midbrain (Grothe and Pecka 2014). Thus, anesthesia should – if at all – only have a decent effect on subcortical computations of ILDs.

Hence, the suppression of frontal positions by anesthesia is probably in large parts the product of disturbed cortical processes. Indeed, the cortex seems to be the major site of action for general anesthetics (Hentschke et al. 2005). The prefrontal cortex has been shown to exert control over auditory processes in the AC (Fritz et al. 2010). Such top-down regulatory processes will be impaired under anesthesia. Furthermore, the AC will lack default inputs from other cortical areas such as visual (Bizley et al. 2007) and somatosensory (Cappe and Barone 2005) cortex. Trimming of cortical activity by means of anesthesia leaves the AC with unmodulated bottom-up ILD computation which results in a preference for

contralateral positions under anesthesia while sparing the representation of frontal positions.

### 4.4.   Anesthesia does not modify spatial tuning width in the AC

Although anesthesia altered the population response as well as the spatial preference of individual cells, no effect of anesthesia on spatial tuning width was observed. This contradicts a previous report from Mickey and Middlebrooks (2003) which describes potentially decreased tuning widths in awake animals, though their study lacks a direct comparison of anesthetized and awake animals. As opposed to their observation my findings do not support the idea of decreased tuning widths in awake animals. Sharpening of tuning was absent on the population level (Figure 11c) as well as on the single-cell level (Figure 11d). The discrepancy between my study and the report from Mickey and Middlebrooks (2003) might be best explained by differences in task engagement. Whereas Mickey and Middlebrooks (2003) had animals reporting the location of a target cue by releasing a key upon target presentation, the animals in my experiments did not have to engage in any task. It is likely that the task requirement in Mickey and Middlebrooks (2003) caused a sharpening of tuning widths above average. Mickey and Middlebrooks (2003) report a decrease of tuning width in the performing state (compared to periods in which animals were idle). Later research from the same laboratory showed that spatial receptive field size indeed decreases with increasing task engagement (Lee and Middlebrooks 2011). For this reason Mickey and Middlebrooks (2003) probably observed sharper tuning when animals were awake. However, if animals are not engaged in any task, it can be assumed that tuning width is not decreased in awake animals.

### 4.5.   The AC lacks a map of auditory space

Inspired by the pivotal work of Knudsen and Konishi (1978) and Knudsen (1982) that reported maps of auditory space in the midbrain auditory nucleus and the optic tectum of the barn owl, many electrophysiologists aimed to determine

such a map in the auditory cortex of mammals as well. Nevertheless, all studies to date continuously failed to report a structured arrangement of neurons coding for auditory space across different species such as the cat (Middlebrooks and Pettigrew 1981; Imig et al. 1990; Rajan et al. 1990a; Clarey et al. 1994), rat (Yao et al. 2013), ferret (Nelken et al. 2008) and monkey (Woods et al. 2006; Remington and Wang 2019). Despite the continuous failure of studies to identify a map of auditory space, the possible existence of such a map could not be entirely excluded. Electrophysiological recordings tend to sample from highly active neurons (Shoham et al. 2006), potentially pool across neurons and only allow for a relatively small sample size. Calcium imaging in contrast provides a less biased approach to obtain data from large populations of neurons, while determining the cortical position of cells with extremely high precision. For instance, recent calcium imaging studies on tonotopy report divergent results from previous microelectrode experiments (Bandyopadhyay et al. 2010; Rothschild et al. 2010). These studies point towards a more scattered distribution of frequency tuning in AC arguing against a smooth tonotopic gradient, which has for a long time been considered to be one of the hallmarks of the AC's functional organization. For all these reasons, calcium imaging seems to be especially suited to probe the existence of an auditory space map, which might have been disregarded by the coarse sampling of previous microelectrode studies. However, research exploiting calcium imaging to address this question has remained scarce. Panniello et al. (2018) did so in anesthetized mice, but in none of the animals studied they could detect a structured arrangement of ILD preferring neurons across the AC. It is unclear if this represents a true absence of an auditory space map, because later research has suggested that sound locations rather than binaural spatial cues are decoded by neurons as early as the level of the primary AC (Wood et al. 2019). Performing calcium imaging in anesthetized mice while applying auditory free field stimulation, my results nevertheless resemble the reports from prior electrophysiological research and only deviate to a small

degree from the finding made by Panniello et al. (2018). As in all publications seeking to identify a map of auditory space, my results yield no evidence for a topographical arrangement of neurons preferring the same best speaker locations (Figure 12). In contrast to Panniello et al. (2018) but in line with several other reports (Middlebrooks and Pettigrew 1981; Imig et al. 1990; Rajan et al. 1990a; Clarey et al. 1994; Nelken et al. 2008; Middlebrooks 2021), I observed a cluster of similar tuned neurons in one anesthetized animal. However, it is possible that in my study and the one performed by Panniello et al. (2018) the application of anesthesia caused the failure to identify a map of auditory space. But probing the existence of a space map in awake animals also did not yield evidence for a topographical arrangement of neurons preferring similar best speaker locations, despite observed local clusters of similar tuned neurons in some animals, indicating absence of an auditory space map also in awake animals. In brief, my observations confirm earlier electrophysiological work that assumed absence of a space map in the AC in mammals (for an extensive review see Middlebrooks 2021). Importantly, lack thereof cannot be explained by the fact that previous research relied heavily on anesthetized preparations, since my results also do not identify a structured arrangement of spatial preference in awake animals. Therefore, the mammalian AC lacks a map of auditory space.

## 4.6. Anesthesia masks the complexity of spatial tuning in the AC

Using automatic classification I identified the preponderance of the following three major classes of neurons (Figure 13a): a class of neurons that showed sharp, clearly circumscribed spatial tuning by exhibiting tuning to one location only (termed *specific*), a class of neurons that displayed simple broad spatial tuning towards two or more neighboring locations (termed *broad*), and a class of neurons that exhibited complex "V" or "M" shaped tuning curves as they had two maxima separated by a through (termed *bilobed*). Despite reports of similar such spatial tuning curves in previous studies (Rajan et al. 1990a; Irvine

et al. 1996; Mrsic-Flogel et al. 2005; Mickey and Middlebrooks 2003; Middlebrooks and Pettigrew 1981; Imig et al. 1990; Rajan et al. 1990b) which suggested the existence of these categories, none of these studies explicitly aimed to categorize tuning curves based on their shapes. My results reveal that in anesthetized as well as in awake animals ~60% of spatially selective neurons fall into one of these categories (Figure 13b). Under both conditions, most of these neurons respond best to one single location (*specific*). However, in the awake condition fewer neurons than in the anesthetized condition were found to exhibit simple broad tuning curves (*broad*). Instead, more neurons had somewhat complex tuning curves as being identified to be *bilobed*. Overall, this indicates that spatial tuning in awake animals is more complex than in anesthetized animals.

### 4.7. Auditory space representation is stable despite noisy single-cell tuning

Performing chronic imaging of the same neurons over multiple weeks, I could reveal that in awake and anesthetized animals single-cell spatial tuning is extremely noisy and dynamic. The majority of neurons gained or lost their spatial selectivity across imaging sessions (Figure 14d) and more than 80% of neurons changed their spatial tuning curves across those sessions (Figure 15a). This observation might appear surprising at first, but recently frequency-tuning of individual AC neurons has been shown to also be highly dynamic (Aschauer et al. 2019). Similar findings have also been made in other brain areas. Performing chronic calcium imaging in the CA1 of freely behaving mice Ziv et al. (2013) report that only a minority of cells (15 - 25%) contributed to place coding in more than one session. Similar observations have been found on the single-cell level in motor cortex (Rokni et al. 2007; Huber et al. 2012) and in the posterior parietal cortex (Driscoll et al. 2017). Taken together, the extreme dynamics of individual single-cell tuning that I have uncovered for spatial tuning in AC provides further evidence that noisy tuning of individual neurons might be a common coding principle in auditory and potentially other higher order sensory cortices (keep in

mind that primary visual cortex and primary somatosensory cortex are synaptically closer to the sensory surface than AC).

The functional role of unstable single-cell tuning however remains elusive. Studying motor cortex Rokni et al. (2007) propose that unstable tuning functions might serve to add noise to representations making them more robust to daily variations in the environment. Just as motor outputs include a strongly stochastic component (e.g. the same movement might vary from trial to trial thus displaying randomness), so are the inputs to the auditory system caused by the environment (e.g. a predator might change his position unpredictably thus forcing constant volatile updates of the encompassing auditory space to elicit the appropriate escape behavior). Ever-changing spatial tuning characteristics of individual cells in the AC could for example help to account for erratic changes in the acoustic environment as well as adjusting the system to sudden changes in attentional or contextual demands.

I have shown that single-cell spatial tuning is highly unstable and that these dynamics might potentially serve to provide the AC with the ability to react with the required flexibility to the daily variations abundant in environmental statistics. But how can the AC maintain a stable percept of auditory space in the light of such a strong variability of spatial tuning on the single-cell level? There is accumulating evidence that stable representations are achieved via stable population responses despite variable single-cell responses. This has been shown for motor cortex (Huber et al. 2012), hippocampus (Ziv et al. 2013), posterior parietal cortex (Driscoll et al. 2017) and recently for frequency tuning in the AC (Aschauer et al. 2019; Romero et al. 2020). Probing the stability of the population code to spatial stimuli, I uncovered that population responses were remarkably stable (Figure 15b). Since the tuning of individual neurons was extremely dynamic, I argue that it is the population code that provides the organism with a stable representation of auditory space. However, changes in behavioral

demands are likely to cause adaptations of the population code. Recording single- and multi-units from cat AC while being engaged in a spatial localization task revealed that up to 44% of units recorded sharpened their receptive field (Lee and Middlebrooks 2011). Furthermore, auditory cortex activity has been shown to be modulated by activity from other sensory areas such as visual cortex (Calvert et al. 1997; Kayser et al. 2007; Kayser et al. 2008). Given the complex interconnectedness of AC and the behavioral need to adjust to ever-changing internal and external contexts the population code itself will likely be in constant flux, constantly optimizing its output.

## 4.8.    Methodological considerations

Chronic *in vivo* two photon calcium imaging relies on calcium indicators to measure neural activity. Due to the slow kinetics of these sensors, calcium imaging lacks high temporal resolution. In addition, this technique struggles to identify individual action potentials because calcium indicators behave in a non-linear fashion making it extremely hard to estimate the number of action potentials elicited. Thus, because calcium imaging provides only an indirect readout of cellular activity, several attempts have been made to infer spikes from the measured calcium transients. Although identification of the underlying spike pattern has improved in recent years (Deneux et al. 2016; Pachitariu et al. 2018), spike inference remains dodgy as the problem it tries to solve is ill-posed. I therefore avoided applying spike inference to my calcium data. Despite these limitations, calcium imaging provides the great advantage of measuring the responses of large populations of neurons without introducing a sampling bias towards highly active cells. In addition, the same cells can be tracked over multiple days, weeks and even months and their exact cortical position can be determined. Thus, calcium imaging is the ultimate tool for tackling questions of population coding and chronic neural stability.

### 4.9.  Implications for future research

In the previous paragraphs I have presented and discussed the results of my thesis. The observations made raise several questions regarding the spatial representation in the AC which should be addressed by future research.

Although in the awake condition animals were non-behaving, the influence of physiological parameters like arousal were not monitored in the present study. As pointed out in the previous section (see section 2.5), arousal (Lin et al. 2019) and motor activity (Schneider and Mooney 2018; Musall et al. 2019) can alter AC activity. Although it remains improbable that these parameters strongly affected my results, future research will need to address this issue to fully rule out potential influences. Body and eye tracking of the pupil could be applied to disentangle the impact of body movement and arousal upon auditory space representation in awake animals. As locomotion has been shown to downregulate sound-evoked responses in AC (Zhou et al. 2014; Kuchibhotla et al. 2017), similar can be postulated for the spatial tuning properties of AC neurons. Intensified levels of arousal (as indexed by pupil dilation) have been found to increase frequency discrimination in mouse AC by increasing covariation of signal and noise correlations (Lin et al. 2019). Likewise, could be expected for spatial tuning of neurons in AC if arousal increases.

By presenting sounds from a horizontal hoop I was able to reveal how auditory space is represented in the AC under naturalistic conditions. Unfortunately, accessing the AC and at the same time maintaining the animal in an upright posture required rotation of the microscope, sampling of auditory space was limited to a range of 120°. As sampling of the full 360° was currently impracticable, updating the design of the horizontal hoop by increasing the range of space sampled will allow it to capture the full granularity that underlies spatial tuning in AC. This especially applies to neurons that show their preferred responses to the ipsilateral or the rear side.

Using an automatic classification approach I was able to group the tuning curves into three major categories based on their shapes. The functional relevance of these categories however remains unclear, which might only become apparent in behaving animals. It might be possible that sharply tuned neurons serve a special function in sound localization behavior by dynamically adjusting their preferred location. Considering the work of Lee and Middlebrooks (2011), broadly tuned neurons can sharpen their receptive fields once animals actively perform sound localization, whereas the behavior of the bilobed ones remains elusive at the moment. Future research might prove fruitful by investigating functional changes in these groups while animals engage in an auditory localization task.

In line with previous research my results also point against the existence of a spatial map in AC. However, at the moment it cannot be fully ruled out that such a map could still be detected in the thalamorecipient layers of the AC. As Panniello et al. (2018), I performed calcium imaging in the supragranular layers of the mouse AC. However, Phillips and Irvine (1983) and Reser et al. (2000) report that clusters of binaural response properties could exist in the thalamorecipient layers of cortex. As long as calcium imaging of neurons in cortical layer 4 is not conducted, the existence of an auditory space map should only be ruled out for the supragranular layers of rodent AC.

Two-photon imaging in the primary visual cortex showed that the pinwheel organization found in higher mammals is absent in rodents (Ohki and Reid 2007). It remains possible that similar applies to AC, i.e. that an auditory space map is absent in rodent AC but does exist in the AC of higher mammals. Therefore, two-photon imaging in higher mammals will be required to probe if a map of auditory space is also absent in those species.

Coding of ILDs in the LSO and ITDs in the MSO exhibits broad tuning with linear spike rate modulation over a wide range of positions. MSO neurons

usually respond best to ITDs corresponding to contralateral positions, whereas LSO neurons tend to favor ILDs corresponding to ipsilateral positions (Grothe et al. 2010). As a result, sound localization has been suggested to be achieved by two opponent hemispherical tuned coding channels each located within a single hemisphere. These models propose that at later stages of the auditory pathway the location of a sound source is determined by comparing the relative activity of these channels (McAlpine et al. 2001; Phillips and Hall 2005; Stecker et al. 2005; Vigneault-MacLean et al. 2007; Grothe et al. 2010; Briley et al. 2013; Grothe and Pecka 2014). It must be noted in this context that the incoherent coding of MSO (contralateral positions) and LSO neurons (ipsilateral positions) is harmonized at the midbrain as LSO neurons target the contralateral midbrain while MSO neurons project to the ipsilateral midbrain. My data shows that in awake animals the majority of AC neurons displays tuning towards the front or to the contralateral side but that the representation of frontal positions is suppressed under anesthesia. Therefore, a third channel tuned towards the midline seems to emerge downstream of the brainstem whose detection is obscured by anesthesia. The existence of such a channel has already been proposed by Dingle et al. (2010) and Briley et al. (2016).

Especially, the functional neural apparatus underlying spatial coding in the mammalian AC still requires further investigation. For example, Dingle et al. (2010) suggested a model that has each hemisphere equipped with three channels (contra, ipsi, midline), but each hemisphere serves sound localization exclusively in the contralateral hemifield. Assuming existence of such a neural implementation, sectioning the corpus callosum should not impair sound localization considerably. However, a unilateral lesion on top should wash out sound localization solely in the contralateral hemifield. Hence, assessing sound localization accuracy prior to and after selective cortical lesions would be vital to

decipher in greater detail the neural machinery of AC that enables sound localization.

Future directions could also investigate the influences of other cortical areas onto space representation in the AC. Research in humans and monkeys has revealed that AC is highly multisensory integrating visual and somatosensory information. Visual acoustic cues alone can activate AC (Calvert et al. 1997; Kayser et al. 2007; Kayser et al. 2008). Furthermore, AC seems to integrate audiovisual (Ghazanfar et al. 2005) and audio-somatosensory (Kayser et al. 2005; Lakatos et al. 2007) information. Also frontal regions have been found to exert control over auditory cortical processes (Fritz et al. 2010). Recently, frontal cortex has been suggested to combine information from visual and AC to guide decision making (Coen et al. 2021). This pool of research shows that AC is highly interconnected with other unimodal and higher order brain regions. The regulating role of frontal cortex on AC could be assessed by lesioning or optogenetically silencing frontal cortex, while animals perform a familiar sound localization task.[1] Simultaneously, calcium imaging recordings could be carried out to identify if neurons adapt their tuning properties if frontal influences are missing. It might be possible that neurons that sharpen their spatial receptive fields during task engagement (Lee and Middlebrooks 2011), lose this property if frontal cortex is dysfunctional. Similar could be done while animals carry out a bimodal localization task. It would be thrilling to see if AC neurons reduce their spatial discriminability if integration of additional sensory input is impaired. For example indication of a water reward by spatially pairing a tone and light stimulus and silencing (or lesioning) visual cortex while simultaneously recording from AC neurons would be a valuable means to test this.

---

[1] Optogenetics allows for temporal and spatial fine-grained optical manipulation of neural circuits by inhibiting or exciting neurons by means of stimulating light-driven effector proteins.

The GECI that I used was expressed under the synapsin 1 promoter. Synapsin is a neuron-specific protein, which is expressed in excitatory and inhibitory neurons (Kügler et al. 2003). Most neurons in the cortex (~80%) are excitatory (White 1989). Thus, the majority of neurons labeled by the indicator were, most likely, to a large part excitatory ones. Whereas one can speculate that most of the processes uncovered by my work are therefore executed by excitatory neurons, no statement about the neuronal cell types involved is possible. Calcium imaging of transgenic mice, which express fluorescent proteins only in very selective subsets of neurons, would allow to dissect which types of cortical neurons contribute most to representations of auditory space.

Although I tried to primarily inject the virus construct into the primary AC, it is hard to restrict my results to primary AC since virus injection was based on the blood vessel pattern. This layout tends to vary across animals, which makes it hard to target the identical positions across animals. Thus it remains possible that the virus was also injected into other subregions of AC. In addition, it cannot be ruled out that the bulk injection method which was applied to inject the virus into the target area caused the virus to spread into other regions of AC and therefore led to transduction of a larger area. Also it is noteworthy that the delineation of mouse AC and its constituting subregions are still under debate (Tsukano et al. 2015). Therefore, it remains an open question how the various subregions of the AC contribute to spatial hearing. Prior to virus injection and/or population calcium imaging, intrinsic optical imaging of AC could be carried out while stimulating animals with pure tones at certain increments. This would allow to subdivide the AC by means of tonotopy more accurately and in the following enable dissecting the roles of AC's individual constituents in spatial coding.

By exploiting electrophysiological recordings from the AC of cats, Lee and Middlebrooks (2011) were able to show that task engagement shapes the

receptive fields of neurons. Their elegant study raises questions on the contextual effects of attention and learning upon single and population spatial coding. This could be addressed by combining two-photon calcium imaging with behavior to monitor AC activity while animals learn to perform a sound localization task. This will not only help to uncover how single neurons and the population code behave while animals learn but also boost our understanding of how neurons respond to task changes once the initial task has been learned. This research will be crucial to uncover how populations of neurons respond to changes in task demands. Naturally, reversible silencing of interhemispheric or frontal connections will help to further dissect the behavior of the circuit and expand our understanding of the coding scheme underlying spatial representation in the AC.

A complementary approach that has in recent years undergone substantial technical improvements is electrophysiology. With the advent of Neuropixels (Jun et al. 2017), and their newest version (Steinmetz et al. 2021), chronic recordings of large populations of neurons with extremely high temporal resolution have become possible. Utilizing this tool to record from awake animals while probing spatial stimulation has the capability to reveal the full wealth of information encoded within large populations of neurons. Functional networks of neurons contributing to representations of auditory space could be identified while at the same time the information carrying role of first spike latency and mean spike rate in spatial coding could be further disentangled (see section 4.2; panoramic code for sound localization).

## 5. CONCLUSIONS

To conclude, by performing chronic two-photon calcium imaging of large populations of neurons in awake and anesthetized animals this thesis identified the effects of anesthesia upon auditory space representation in the mouse AC. Firstly, I observed that spatial sensitivity is impaired under anesthesia. Secondly, my results support the notion that AC lacks a topographic map of auditory space. Thirdly, I could confirm that anesthesia suppresses the representation of frontal locations. Fourthly, chronic imaging revealed that spatial tuning of individual cells is extremely dynamic, whereas the population response is exceptionally stationary thus likely granting AC with a stable representation of auditory space.

# PUBLICATION BIBLIOGRAPHY

Aschauer, D. F.; Eppler, J.; Ewig, L.; Chambers, A.; Pokorny, C.; Kaschube, M.; Rumpel, S. (2019): A Basis Set of Elementary Operations Captures Recombination of Neocortical Cell Assemblies During Basal Conditions and Learning. In *SSRN Journal*. DOI: 10.2139/ssrn.3438457.

Averbeck, B. B.; Latham, P. E.; Pouget, A. (2006): Neural correlations, population coding and computation. In *Nature reviews. Neuroscience* 7 (5), pp. 358–366. DOI: 10.1038/nrn1888.

Bandyopadhyay, S.; Shamma, S. A.; Kanold, P. O. (2010): Dichotomy of functional organization in the mouse auditory cortex. In *Nature neuroscience* 13 (3), pp. 361–368. DOI: 10.1038/nn.2490.

Beckius, G. E.; Batra, R.; Oliver, D. L. (1999): Axons from Anteroventral Cochlear Nucleus that Terminate in Medial Superior Olive of Cat: Observations Related to Delay Lines. In *J. Neurosci.* 19 (8), pp. 3146–3161. DOI: 10.1523/JNEUROSCI.19-08-03146.1999.

Behrens, D.; Klump, G. M. (2016): Comparison of mouse minimum audible angle determined in prepulse inhibition and operant conditioning procedures. In *Hearing research* 333, pp. 167–178. DOI: 10.1016/j.heares.2016.01.011.

Bizley, J. K.; Nodal, F. R.; Bajo, V. M.; Nelken, I.; King, A. J. (2007): Physiological and anatomical evidence for multisensory interactions in auditory cortex. In *Cerebral cortex (New York, N.Y.: 1991)* 17 (9), pp. 2172–2189. DOI: 10.1093/cercor/bhl128.

Brand, A.; Behrend, O.; Marquardt, T.; McAlpine, D.; Grothe, B. (2002): Precise inhibition is essential for microsecond interaural time difference coding. In *Nature* 417 (6888), pp. 543–547. DOI: 10.1038/417543a.

Briley, P. M.; Goman, A. M.; Summerfield, A. Q. (2016): Physiological Evidence for a Midline Spatial Channel in Human Auditory Cortex. In *Journal of the Association for Research in Otolaryngology: JARO* 17 (4), pp. 331–340. DOI: 10.1007/s10162-016-0571-y.

Briley, P. M.; Kitterick, P. T.; Summerfield, A. Q. (2013): Evidence for opponent process analysis of sound source location in humans. In *Journal of the Association for Research in Otolaryngology: JARO* 14 (1), pp. 83–101. DOI: 10.1007/s10162-012-0356-x.

Brugge, J. F.; Reale, R. A.; Hind, J. E. (1996): The Structure of Spatial Receptive Fields of Neurons in Primary Auditory Cortex of the Cat. In *J. Neurosci.* 16 (14), pp. 4420–4437. DOI: 10.1523/JNEUROSCI.16-14-04420.1996.

Calvert, G. A.; Bullmore, E. T.; Brammer, M. J.; Campbell, R.; Williams, S. C.; McGuire, P. K. et al. (1997): Activation of auditory cortex during silent lipreading. In *Science (New York, N.Y.)* 276 (5312), pp. 593–596. DOI: 10.1126/science.276.5312.593.

Cappe, C.; Barone, P. (2005): Heteromodal connections supporting multisensory integration at low levels of cortical processing in the monkey. In *The European journal of neuroscience* 22 (11), pp. 2886–2902. DOI: 10.1111/j.1460-9568.2005.04462.x.

Carr, C. E.; Konishi, M. (1988): Axonal delay lines for time measurement in the owl's brainstem. In *Proceedings of the National Academy of Sciences of the United States of America* 85 (21), pp. 8311–8315. DOI: 10.1073/pnas.85.21.8311.

Carr, C. E.; Konishi, M. (1990): A circuit for detection of interaural time differences in the brain stem of the barn owl. In *J. Neurosci.* 10 (10), pp. 3227–3246. DOI: 10.1523/JNEUROSCI.10-10-03227.1990.

Chalfie, M.; Tu, Y.; Euskirchen, G.; Ward, W. W.; Prasher, D. C. (1994): Green fluorescent protein as a marker for gene expression. In *Science (New York, N.Y.)* 263 (5148), pp. 802–805. DOI: 10.1126/science.8303295.

Chen, T.; Wardill, T. J.; Sun, Y.; Pulver, S. R.; Renninger, S. L.; Baohan, A. et al. (2013): Ultrasensitive fluorescent proteins for imaging neuronal activity. In *Nature* 499 (7458), pp. 295–300. DOI: 10.1038/nature12354.

Cheung, S. W.; Nagarajan, S. S.; Bedenbaugh, P. H.; Schreiner, C. E.; Wang, X.; Wong, A. (2001): Auditory cortical neuron response differences under isoflurane versus pentobarbital anesthesia. In *Hearing research* 156 (1-2), pp. 115–127. DOI: 10.1016/S0378-5955(01)00272-6.

Clack, J. A. (1997): The evolution of tetrapod ears and the fossil record. In *Brain, behavior and evolution* 50 (4), pp. 198–212. DOI: 10.1159/000113334.

Clarey, J. C.; Barone, P.; Imig, T. J. (1994): Functional organization of sound direction and sound pressure level in primary auditory cortex of the cat. In *Journal of neurophysiology* 72 (5), pp. 2383–2405. DOI: 10.1152/jn.1994.72.5.2383.

Coen, P.; Sit, T. P.H.; Wells, M. J.; Carandini, M.; Harris, K. D. (2021): Mouse frontal cortex mediates additive multisensory decisions. DOI: 10.1101/2021.04.26.441250.

Cohen, M. R.; Kohn, A. (2011): Measuring and interpreting neuronal correlations. In *Nature neuroscience* 14 (7), pp. 811–819. DOI: 10.1038/nn.2842.

Dahmen, J. C.; Keating, P.; Nodal, F. R.; Schulz, A. L.; King, A. J. (2010): Adaptation to stimulus statistics in the perception and neural representation of auditory space. In *Neuron* 66 (6), pp. 937–948. DOI: 10.1016/j.neuron.2010.05.018.

Darwin, C. (1859): On the origin of species.

Deneux, T.; Kaszas, A.; Szalay, G.; Katona, G.; Lakner, T.; Grinvald, A. et al. (2016): Accurate spike estimation from noisy calcium signals for ultrafast three-dimensional imaging of large neuronal populations in vivo. In *Nature communications* 7, p. 12190. DOI: 10.1038/ncomms12190.

Denk, W.; Strickler, J. H.; Webb, W. W. (1990): Two-photon laser scanning fluorescence microscopy. In *Science (New York, N.Y.)* 248 (4951), pp. 73–76. DOI: 10.1126/science.2321027.

Dingle, R. N.; Hall, S. E.; Phillips, D. P. (2010): A midline azimuthal channel in human spatial hearing. In *Hearing research* 268 (1-2), pp. 67–74. DOI: 10.1016/j.heares.2010.04.017.

Driscoll, L. N.; Pettit, N. L.; Minderer, M.; Chettih, S. N.; Harvey, C. D. (2017): Dynamic Reorganization of Neuronal Activity Patterns in Parietal Cortex. In *Cell* 170 (5), 986-999.e16. DOI: 10.1016/j.cell.2017.07.021.

Eggermont, J. J. (1998): Azimuth coding in primary auditory cortex of the cat. II. Relative latency and interspike interval representation. In *Journal of neurophysiology* 80 (4), pp. 2151–2161. DOI: 10.1152/jn.1998.80.4.2151.

Ellenbroek, B.; Youn, J. (2016): Rodent models in neuroscience research: is it a rat race? In *Disease models & mechanisms* 9 (10), pp. 1079–1087. DOI: 10.1242/dmm.026120.

Fritz, J. B.; David, S. V.; Radtke-Schuller, S.; Yin, P.; Shamma, S. A. (2010): Adaptive, behaviorally gated, persistent encoding of task-relevant auditory information in ferret frontal cortex. In *Nature neuroscience* 13 (8), pp. 1011–1019. DOI: 10.1038/nn.2598.

Furukawa, S.; Middlebrooks, J. C. (2002): Cortical representation of auditory space: information-bearing features of spike patterns. In *Journal of neurophysiology* 87 (4), pp. 1749–1762. DOI: 10.1152/jn.00491.2001.

Gaese, B. H.; Ostwald, J. (2001): Anesthesia changes frequency tuning of neurons in the rat primary auditory cortex. In *Journal of neurophysiology* 86 (2), pp. 1062–1066. DOI: 10.1152/jn.2001.86.2.1062.

Getzmann, S. (2004): Spatial discrimination of sound sources in the horizontal plane following an adapter sound. In *Hearing research* 191 (1-2), pp. 14–20. DOI: 10.1016/j.heares.2003.12.020.

Ghazanfar, A. A.; Maier, J. X.; Hoffman, K. L.; Logothetis, N. K. (2005): Multisensory integration of dynamic faces and voices in rhesus monkey auditory cortex. In *J. Neurosci.* 25 (20), pp. 5004–5012. DOI: 10.1523/JNEUROSCI.0799-05.2005.

Göppert-Mayer, M. (1931): Über Elementarakte mit zwei Quantensprüngen (401).

Grasshoff, C.; Antkowiak, B. (2006): Effects of isoflurane and enflurane on GABAA and glycine receptors contribute equally to depressant actions on spinal ventral horn neurones in rats. In *British journal of anaesthesia* 97 (5), pp. 687–694. DOI: 10.1093/bja/ael239.

Grothe, B.; Sanes, D. H. (1993): Bilateral inhibition by glycinergic afferents in the medial superior olive. In *Journal of neurophysiology* 69 (4), pp. 1192–1196. DOI: 10.1152/jn.1993.69.4.1192.

Grothe, B.; Sanes, D. H. (1994): Synaptic inhibition influences the temporal coding properties of medial superior olivary neurons: an in vitro study. In *J. Neurosci.* 14 (3), pp. 1701–1709. DOI: 10.1523/JNEUROSCI.14-03-01701.1994.

Grothe, B. (2003): New roles for synaptic inhibition in sound localization. In *Nature reviews. Neuroscience* 4 (7), pp. 540–550. DOI: 10.1038/nrn1136.

Grothe, B.; Pecka, M. (2014): The natural history of sound localization in mammals--a story of neuronal inhibition. In *Frontiers in neural circuits* 8, p. 116. DOI: 10.3389/fncir.2014.00116.

Grothe, B.; Pecka, M. McAlpine, D. (2010): Mechanisms of sound localization in mammals. In *Physiological reviews* 90 (3), pp. 983–1012. DOI: 10.1152/physrev.00026.2009.

Heffner, H.; Masterton, B. (1975): Contribution of auditory cortex to sound localization in the monkey (Macaca mulatta). In *Journal of neurophysiology* 38 (6), pp. 1340–1358. DOI: 10.1152/jn.1975.38.6.1340.

Heffner, H. E.; Heffner, R. S. (1990): Effect of bilateral auditory cortex lesions on sound localization in Japanese macaques. In *Journal of neurophysiology* 64 (3), pp. 915–931. DOI: 10.1152/jn.1990.64.3.915.

Heffner, H.; Masterton, B. (1980): Hearing in Glires: Domestic rabbit, cotton rat, feral house mouse, and kangaroo rat. In *The Journal of the Acoustical Society of America* 68 (6), pp. 1584–1599. DOI: 10.1121/1.385213.

Heffner, H. E.; Heffner, R. S. (2007): Hearing ranges of laboratory animals. In *Journal of the American Association for Laboratory Animal Science: JAALAS* 46 (1), pp. 20–22.

Heffner, R. S.; Koay, G.; Heffner, H. E. (2001): Focus: Sound-Localization Acuity Changes with Age in C57BL/6J Mice. In James F. Willott (Ed.): Handbook of Mouse Auditory Research: CRC Press, pp. 31–35.

Helmchen, F.; Denk, W. (2005): Deep tissue two-photon microscopy. In *Nature methods* 2 (12), pp. 932–940. DOI: 10.1038/NMETH818.

Hentschke, H.; Schwarz, C.; Antkowiak, B. (2005): Neocortex is the major target of sedative concentrations of volatile anaesthetics: strong depression of firing rates and increase of GABA A receptor-mediated inhibition. In *European Journal of Neuroscience* 21 (1), pp. 93–102. DOI: 10.1111/j.1460-9568.2004.03843.x.

Huang, A. Y.; May, B. J. (1996): Spectral cues for sound localization in cats: effects of frequency domain on minimum audible angles in the median and horizontal planes. In *The Journal of the Acoustical Society of America* 100 (4 Pt 1), pp. 2341–2348. DOI: 10.1121/1.417943.

Huber, D.; Gutnisky, D. A.; Peron, S.; O'Connor, D. H.; Wiegert, J. S.; Tian, L. et al. (2012): Multiple dynamic representations in the motor cortex during sensorimotor learning. In *Nature* 484 (7395), pp. 473–478. DOI: 10.1038/nature11039.

Imig, T. J.; Irons, W. A.; Samson, F. R. (1990): Single-unit selectivity to azimuthal direction and sound pressure level of noise bursts in cat high-frequency primary auditory cortex. In *Journal of neurophysiology* 63 (6), pp. 1448–1466. DOI: 10.1152/jn.1990.63.6.1448.

Irvine, D. R.; Rajan, R.; Aitkin, L. M. (1996): Sensitivity to interaural intensity differences of neurons in primary auditory cortex of the cat. I. types of sensitivity and effects of variations in sound pressure level. In *Journal of neurophysiology* 75 (1), pp. 75–96. DOI: 10.1152/jn.1996.75.1.75.

Ison, J. R.; Allen, P. D.; O'Neill, W. E. (2007): Age-related hearing loss in C57BL/6J mice has both frequency-specific and non-frequency-specific components that produce a hyperacusis-like exaggeration of the acoustic startle reflex. In *Journal of the Association for Research in Otolaryngology: JARO* 8 (4), pp. 539–550. DOI: 10.1007/s10162-007-0098-3.

Jeffress, L. A. (1948): A place theory of sound localization. In *Journal of comparative and physiological psychology* 41 (1), pp. 35–39. DOI: 10.1037/h0061495.

Jenkins, W. M.; Masterton, R. B. (1982): Sound localization: effects of unilateral lesions in central auditory system. In *Journal of neurophysiology* 47 (6), pp. 987–1016. DOI: 10.1152/jn.1982.47.6.987.

Jenkins, W. M.; Merzenich, M. M. (1984): Role of cat primary auditory cortex for sound-localization behavior. In *Journal of neurophysiology* 52 (5), pp. 819–847. DOI: 10.1152/jn.1984.52.5.819.

Joachimsthaler, B.; Uhlmann, M.; Miller, F.; Ehret, G.; Kurt, S. (2014): Quantitative analysis of neuronal response properties in primary and higher-order auditory cortical fields of awake house mice (Mus musculus). In *The European journal of neuroscience* 39 (6), pp. 904–918. DOI: 10.1111/ejn.12478.

Joris, P. X.; Smith, P. H.; Yin, Tom C.T (1998): Coincidence Detection in the Auditory System. In *Neuron* 21 (6), pp. 1235–1238. DOI: 10.1016/S0896-6273(00)80643-1.

Jun, J. J.; Steinmetz, N. A.; Siegle, J. H.; Denman, D. J.; Bauza, M.; Barbarits, B. et al. (2017): Fully integrated silicon probes for high-density recording of neural activity. In *Nature* 551 (7679), pp. 232–236. DOI: 10.1038/nature24636.

Kaiser, W.; Garrett, C. G. B. (1961): Two-Photon Excitation in Ca F2 : Eu2+. In *Phys. Rev. Lett.* 7 (6), pp. 229–231. DOI: 10.1103/PhysRevLett.7.229.

Kato, H. K.; Gillet, S. N.; Isaacson, J. S. (2015): Flexible Sensory Representations in Auditory Cortex Driven by Behavioral Relevance. In *Neuron* 88 (5), pp. 1027–1039. DOI: 10.1016/j.neuron.2015.10.024.

Kayser, C.; Petkov, C. I.; Augath, M.; Logothetis, N. K. (2005): Integration of touch and sound in auditory cortex. In *Neuron* 48 (2), pp. 373–384. DOI: 10.1016/j.neuron.2005.09.018.

Kayser, C.; Petkov, C. I.; Augath, M.; Logothetis, N. K. (2007): Functional imaging reveals visual modulation of specific fields in auditory cortex. In *J. Neurosci.* 27 (8), pp. 1824–1835. DOI: 10.1523/JNEUROSCI.4737-06.2007.

Kayser, C.; Petkov, C. I.; Logothetis, N. K. (2008): Visual modulation of neurons in auditory cortex. In *Cerebral cortex (New York, N.Y. : 1991)* 18 (7), pp. 1560–1574. DOI: 10.1093/cercor/bhm187.

Knudsen, E. I. (1982): Auditory and visual maps of space in the optic tectum of the owl. In *J. Neurosci.* 2 (9), pp. 1177–1194. DOI: 10.1523/JNEUROSCI.02-09-01177.1982.

Knudsen, E. I.; Konishi, M. (1978): A neural map of auditory space in the owl. In *Science (New York, N.Y.)* 200 (4343), pp. 795–797. DOI: 10.1126/science.644324.

Kuchibhotla, K. V.; Gill, J. V.; Lindsay, G. W.; Papadoyannis, E. S.; Field, R. E.; Sten, T. A. Hindmarsh et al. (2017): Parallel processing by cortical inhibition enables context-dependent behavior. In *Nature neuroscience* 20 (1), pp. 62–71. DOI: 10.1038/nn.4436.

Kügler, S.; Kilic, E.; Bähr, M. (2003): Human synapsin 1 gene promoter confers highly neuron-specific long-term transgene expression from an adenoviral vector in the adult rat brain depending on the transduced area. In *Gene therapy* 10 (4), pp. 337–347. DOI: 10.1038/sj.gt.3301905.

Lakatos, P.; Chen, C.; O'Connell, M. N.; Mills, A.; Schroeder, C. E. (2007): Neuronal oscillations and multisensory interaction in primary auditory cortex. In *Neuron* 53 (2), pp. 279–292. DOI: 10.1016/j.neuron.2006.12.011.

Lauer, A. M.; Slee, S. J.; May, B. J. (2011): Acoustic basis of directional acuity in laboratory mice. In *Journal of the Association for Research in Otolaryngology: JARO* 12 (5), pp. 633–645. DOI: 10.1007/s10162-011-0279-y.

Lee, C.; Middlebrooks, J. C. (2011): Auditory cortex spatial sensitivity sharpens during task performance. In *Nature neuroscience* 14 (1), pp. 108–114. DOI: 10.1038/nn.2713.

Lin, P.; Asinof, S. K.; Edwards, N. J.; Isaacson, J. S. (2019): Arousal regulates frequency tuning in primary auditory cortex. In *Proceedings of the National Academy of Sciences of the United States of America* 116 (50), pp. 25304–25310. DOI: 10.1073/pnas.1911383116.

Lingner, A.; Pecka, M.; Leibold, C.; Grothe, B. (2018): A novel concept for dynamic adjustment of auditory space. In *Scientific reports* 8 (1), p. 8335. DOI: 10.1038/s41598-018-26690-0.

Luo, L. (2015): Principles of Neurobiology: Garland Science.

Magnusson, A. K.; Park, T. J.; Pecka, M.; Grothe, B.; Koch, U. (2008): Retrograde GABA signaling adjusts sound localization by balancing excitation and

inhibition in the brainstem. In *Neuron* 59 (1), pp. 125–137. DOI: 10.1016/j.neuron.2008.05.011.

Malhotra, S.; Hall, A. J.; Lomber, S. G. (2004): Cortical control of sound localization in the cat: unilateral cooling deactivation of 19 cerebral areas. In *Journal of neurophysiology* 92 (3), pp. 1625–1643. DOI: 10.1152/jn.01205.2003.

Malhotra, S.; Stecker, G. C.; Middlebrooks, J. C.; Lomber, S. G. (2008): Sound localization deficits during reversible deactivation of primary auditory cortex and/or the dorsal zone. In *Journal of neurophysiology* 99 (4), pp. 1628–1642. DOI: 10.1152/jn.01228.2007.

Martin, R. L.; Webster, W. R. (1987): The auditory spatial acuity of the domestic cat in the interaural horizontal and median vertical planes. In *Hearing research* 30 (2-3), pp. 239–252. DOI: 10.1016/0378-5955(87)90140-7.

Masterton, B.; Diamond, I. T.; Harrison, J. M.; Beecher, M. D. (1967): Medial superior olive and sound localization. In *Science (New York, N.Y.)* 155 (3770), pp. 1696–1697. DOI: 10.1126/science.155.3770.1696-a.

McAlpine, D.; Jiang, D.; Palmer, A. R. (2001): A neural code for low-frequency sound localization in mammals. In *Nature neuroscience* 4 (4), pp. 396–401. DOI: 10.1038/86049.

McGinley, M. J.; Vinck, M.; Reimer, J.; Batista-Brito, R.; Zagha, E.; Cadwell, C. R. et al. (2015): Waking State: Rapid Variations Modulate Neural and Behavioral Responses. In *Neuron* 87 (6), pp. 1143–1161. DOI: 10.1016/j.neuron.2015.09.012.

Mickey, B. J.; Middlebrooks, J. C. (2003): Representation of Auditory Space by Cortical Neurons in Awake Cats. In *J. Neurosci.* 23 (25), pp. 8649–8663. DOI: 10.1523/JNEUROSCI.23-25-08649.2003.

Middlebrooks, J. C.; Clock, A. E.; Xu, L.; Green, D. M. (1994): A panoramic code for sound location by cortical neurons. In *Science (New York, N.Y.)* 264 (5160), pp. 842–844. DOI: 10.1126/science.8171339.

Middlebrooks, J. C.; Pettigrew, J. D. (1981): Functional classes of neurons in primary auditory cortex of the cat distinguished by sensitivity to sound location. In *J. Neurosci.* 1 (1), pp. 107–120. DOI: 10.1523/JNEUROSCI.01-01-00107.1981.

Middlebrooks, J. C.; Xu, L.; Eddins, A. C.; Green, D. M. (1998): Codes for sound-source location in nontonotopic auditory cortex. In *Journal of neurophysiology* 80 (2), pp. 863–881. DOI: 10.1152/jn.1998.80.2.863.

Middlebrooks, J. C. (2021): A Search for a Cortical Map of Auditory Space. In *J. Neurosci.* DOI: 10.1523/JNEUROSCI.0501-21.2021.

Mills, A. W. (1958): On the Minimum Audible Angle. In *The Journal of the Acoustical Society of America* 30 (4), pp. 237–246. DOI: 10.1121/1.1909553.

Mrsic-Flogel, T. D.; King, A. J.; Schnupp, J. W. H. (2005): Encoding of virtual acoustic space stimuli by neurons in ferret primary auditory cortex. In *Journal of neurophysiology* 93 (6), pp. 3489–3503. DOI: 10.1152/jn.00748.2004.

Musall, S.; Kaufman, M. T.; Juavinett, A. L.; Gluf, S.; Churchland, A. K. (2019): Single-trial neural dynamics are dominated by richly varied movements. In *Nature neuroscience* 22 (10), pp. 1677–1686. DOI: 10.1038/s41593-019-0502-4.

Nakai, J.; Ohkura, M.; Imoto, K. (2001): A high signal-to-noise Ca(2+) probe composed of a single green fluorescent protein. In *Nature biotechnology* 19 (2), pp. 137–141. DOI: 10.1038/84397.

Nelken, I.; Bizley, J. K.; Nodal, F. R.; Ahmed, B.; King, A. J.; Schnupp, J. W. H. (2008): Responses of auditory cortex to complex stimuli: functional organization revealed using intrinsic optical signals. In *Journal of neurophysiology* 99 (4), pp. 1928–1941. DOI: 10.1152/jn.00469.2007.

Noda, T.; Takahashi, H. (2015): Anesthetic effects of isoflurane on the tonotopic map and neuronal population activity in the rat auditory cortex. In *The European journal of neuroscience* 42 (6), pp. 2298–2311. DOI: 10.1111/ejn.13007.

Ohki, K.; Reid, R. C. (2007): Specificity and randomness in the visual cortex. In *Current opinion in neurobiology* 17 (4), pp. 401–407. DOI: 10.1016/j.conb.2007.07.007.

Overholt, E. M.; Rubel, E. W.; Hyson, R. L. (1992): A circuit for coding interaural time differences in the chick brainstem. In *J. Neurosci.* 12 (5), pp. 1698–1708. DOI: 10.1523/JNEUROSCI.12-05-01698.1992.

Pachitariu, M.; Stringer, C.; Harris, K. D. (2018): Robustness of Spike Deconvolution for Neuronal Calcium Imaging. In *J. Neurosci.* 38 (37), pp. 7976–7985. DOI: 10.1523/JNEUROSCI.3339-17.2018.

Panniello, M.; King, A. J.; Dahmen, J. C.; Walker, K. M. M. (2018): Local and Global Spatial Organization of Interaural Level Difference and Frequency Preferences in Auditory Cortex. In *Cerebral cortex (New York, N.Y. : 1991)* 28 (1), pp. 350–369. DOI: 10.1093/cercor/bhx295.

Park, T. J.; Brand, A.; Koch, U.; Ikebuchi, M.; Grothe, B. (2008): Dynamic changes in level influence spatial coding in the lateral superior olive. In *Hearing research* 238 (1-2), pp. 58–67. DOI: 10.1016/j.heares.2007.10.009.

Park, T. J.; Klug, A.; Holinstat, M.; Grothe, B. (2004): Interaural level difference processing in the lateral superior olive and the inferior colliculus. In *Journal of neurophysiology* 92 (1), pp. 289–301. DOI: 10.1152/jn.00961.2003.

Parks, T. N.; Rubel, E. W. (1975): Organization and development of brain stem auditory nuclei of the chicken: organization of projections from n. magnocellularis to n. laminaris. In *The Journal of comparative neurology* 164 (4), pp. 435–448. DOI: 10.1002/cne.901640404.

Pecka, M.; Brand, A.; Behrend, O.; Grothe, B. (2008): Interaural time difference processing in the mammalian medial superior olive: the role of glycinergic inhibition. In *J. Neurosci.* 28 (27), pp. 6914–6925. DOI: 10.1523/JNEUROSCI.1660-08.2008.

Phillips, D. P.; Irvine, D. R. (1983): Some features of binaural input to single neurons in physiologically defined area AI of cat cerebral cortex. In *Journal of neurophysiology* 49 (2), pp. 383–395. DOI: 10.1152/jn.1983.49.2.383.

Phillips, D. P.; Hall, S. E. (2005): Psychophysical evidence for adaptation of central auditory processors for interaural differences in time and level. In *Hearing research* 202 (1-2), pp. 188–199. DOI: 10.1016/j.heares.2004.11.001.

Pologruto, T. A.; Sabatini, B. L.; Svoboda, K. (2003): ScanImage: flexible software for operating laser scanning microscopes. In *Biomedical engineering online* 2, p. 13. DOI: 10.1186/1475-925X-2-13.

Radziwon, K. E.; June, K. M.; Stolzberg, D. J.; Xu-Friedman, M. A.; Salvi, R. J.; Dent, M. L. (2009): Behaviorally measured audiograms and gap detection thresholds in CBA/CaJ mice. In *Journal of comparative physiology. A, Neuroethology, sensory, neural, and behavioral physiology* 195 (10), pp. 961–969. DOI: 10.1007/s00359-009-0472-1.

Rajan, R.; Aitkin, L. M.; Irvine, D. R. (1990a): Azimuthal sensitivity of neurons in primary auditory cortex of cats. II. Organization along frequency-band strips. In *Journal of neurophysiology* 64 (3), pp. 888–902. DOI: 10.1152/jn.1990.64.3.888.

Rajan, R.; Aitkin, L. M.; Irvine, D. R.; McKay, J. (1990b): Azimuthal sensitivity of neurons in primary auditory cortex of cats. I. Types of sensitivity and the effects of variations in stimulus parameters. In *Journal of neurophysiology* 64 (3), pp. 872–887. DOI: 10.1152/jn.1990.64.3.872.

Rayleigh (1907): XII. On our perception of sound direction. In *The London, Edinburgh, and Dublin Philosophical Magazine and Journal of Science* 13 (74), pp. 214–232. DOI: 10.1080/14786440709463595.

Remington, E. D.; Wang, X. (2019): Neural Representations of the Full Spatial Field in Auditory Cortex of Awake Marmoset (Callithrix jacchus). In *Cerebral cortex (New York, N.Y. : 1991)* 29 (3), pp. 1199–1216. DOI: 10.1093/cercor/bhy025.

Reser, D. H.; Fishman, Y. I.; Arezzo, J. C.; Steinschneider, M. (2000): Binaural interactions in primary auditory cortex of the awake macaque. In *Cerebral cortex (New York, N.Y. : 1991)* 10 (6), pp. 574–584. DOI: 10.1093/cercor/10.6.574.

Ries, C. R.; Puil, E. (1999): Mechanism of anesthesia revealed by shunting actions of isoflurane on thalamocortical neurons. In *Journal of neurophysiology* 81 (4), pp. 1795–1801. DOI: 10.1152/jn.1999.81.4.1795.

Rokni, U.; Richardson, A. G.; Bizzi, E.; Seung, H. S. (2007): Motor learning with unstable neural representations. In *Neuron* 54 (4), pp. 653–666. DOI: 10.1016/j.neuron.2007.04.030.

Romero, S.; Hight, A. E.; Clayton, K. K.; Resnik, J.; Williamson, R. S.; Hancock, K. E.; Polley, D. B. (2020): Cellular and Widefield Imaging of Sound Frequency Organization in Primary and Higher Order Fields of the Mouse Auditory Cortex. In *Cerebral cortex (New York, N.Y.: 1991)* 30 (3), pp. 1603–1622. DOI: 10.1093/cercor/bhz190.

Rosowski, J. J.; Graybeal, A. (1991): What did Morganucodon hear? In *Zoological Journal of the Linnean Society* 101 (2), pp. 131–168. DOI: 10.1111/j.1096-3642.1991.tb00890.x.

Rothschild, G.; Nelken, I.; Mizrahi, A. (2010): Functional organization and population dynamics in the mouse primary auditory cortex. In *Nature neuroscience* 13 (3), pp. 353–360. DOI: 10.1038/nn.2484.

Schneider, D. M.; Mooney, R. (2018): How Movement Modulates Hearing. In *Annual review of neuroscience* 41, pp. 553–572. DOI: 10.1146/annurev-neuro-072116-031215.

Schnupp, J. W.; King, A. J. (1997): Coding for auditory space in the nucleus of the brachium of the inferior colliculus in the ferret. In *Journal of neurophysiology* 78 (5), pp. 2717–2731. DOI: 10.1152/jn.1997.78.5.2717.

Shoham, S.; O'Connor, D. H.; Segev, R. (2006): How silent is the brain: is there a "dark matter" problem in neuroscience? In *Journal of comparative physiology.*

*A, Neuroethology, sensory, neural, and behavioral physiology* 192 (8), pp. 777–784. DOI: 10.1007/s00359-006-0117-6.

Smith, A. L.; Parsons, C. H.; Lanyon, R. G.; Bizley, J. K.; Akerman, C. J.; Baker, G. E. et al. (2004): An investigation of the role of auditory cortex in sound localization using muscimol-releasing Elvax. In *The European journal of neuroscience* 19 (11), pp. 3059–3072. DOI: 10.1111/j.0953-816X.2004.03379.x.

Smith, P. H.; Joris, P. X.; Yin, T. C. (1993): Projections of physiologically characterized spherical bushy cell axons from the cochlear nucleus of the cat: evidence for delay lines to the medial superior olive. In *The Journal of comparative neurology* 331 (2), pp. 245–260. DOI: 10.1002/cne.903310208.

Stange, A.; Myoga, M. H.; Lingner, A.; Ford, M. C.; Alexandrova, O.; Felmy, F. et al. (2013): Adaptation in sound localization: from GABA(B) receptor-mediated synaptic modulation to perception. In *Nature neuroscience* 16 (12), pp. 1840–1847. DOI: 10.1038/nn.3548.

Stecker, G. C.; Harrington, I. A.; Middlebrooks, J. C. (2005): Location coding by opponent neural populations in the auditory cortex. In *PLoS biology* 3 (3), e78. DOI: 10.1371/journal.pbio.0030078.

Steinmetz, N. A.; Aydin, C.; Lebedeva, A.; Okun, M.; Pachitariu, M.; Bauza, M. et al. (2021): Neuropixels 2.0: A miniaturized high-density probe for stable, long-term brain recordings. In *Science (New York, N.Y.)* 372 (6539). DOI: 10.1126/science.abf4588.

Tollin, D. J.; Yin, T. C. T. (2002): The Coding of Spatial Location by Single Units in the Lateral Superior Olive of the Cat. I. Spatial Receptive Fields in Azimuth. In *J. Neurosci.* 22 (4), pp. 1454–1467. DOI: 10.1523/JNEUROSCI.22-04-01454.2002.

Tsukano, H.; Horie, M.; Bo, T.; Uchimura, A.; Hishida, R.; Kudoh, M. et al. (2015): Delineation of a frequency-organized region isolated from the mouse primary auditory cortex. In *Journal of neurophysiology* 113 (7), pp. 2900–2920. DOI: 10.1152/jn.00932.2014.

Vigneault-MacLean, B. K.; Hall, S. E.; Phillips, D. P. (2007): The effects of lateralized adaptors on lateral position judgements of tones within and across frequency channels. In *Hearing research* 224 (1-2), pp. 93–100. DOI: 10.1016/j.heares.2006.12.001.

White, E. L. (1989): Cortical Circuits. Boston, MA: Birkhäuser Boston.

Wood, K. C.; Town, S. M.; Bizley, J. K. (2019): Neurons in primary auditory cortex represent sound source location in a cue-invariant manner. In *Nature communications* 10 (1), p. 3019. DOI: 10.1038/s41467-019-10868-9.

Woods, T. M.; Lopez, S. E.; Long, J. H.; Rahman, J. E.; Recanzone, G. H. (2006): Effects of stimulus azimuth and intensity on the single-neuron activity in the auditory cortex of the alert macaque monkey. In *Journal of neurophysiology* 96 (6), pp. 3323–3337. DOI: 10.1152/jn.00392.2006.

Yao, J. D.; Bremen, P.; Middlebrooks, J. C. (2013): Rat primary auditory cortex is tuned exclusively to the contralateral hemifield. In *Journal of neurophysiology* 110 (9), pp. 2140–2151. DOI: 10.1152/jn.00219.2013.

Yin, T. C.; Chan, J. C. (1990): Interaural time sensitivity in medial superior olive of cat. In *Journal of neurophysiology* 64 (2), pp. 465–488. DOI: 10.1152/jn.1990.64.2.465.

Zheng, Q. Y.; Johnson, K. R.; Erway, L. C. (1999): Assessment of hearing in 80 inbred strains of mice by ABR threshold analyses. In *Hearing research* 130 (1-2), pp. 94–107. DOI: 10.1016/s0378-5955(99)00003-9.

Zhou, M.; Liang, F.; Xiong, X. R.; Li, L.; Li, H.; Xiao, Z. et al. (2014): Scaling down of balanced excitation and inhibition by active behavioral states in auditory cortex. In *Nature neuroscience* 17 (6), pp. 841–850. DOI: 10.1038/nn.3701.

Zhou, Y.; Wang, X. (2012): Level dependence of spatial processing in the primate auditory cortex. In *Journal of neurophysiology* 108 (3), pp. 810–826. DOI: 10.1152/jn.00500.2011.

Ziv, Y.; Burns, L. D.; Cocker, E. D.; Hamel, E. O.; Ghosh, K. K.; Kitch, L. J. et al. (2013): Long-term dynamics of CA1 hippocampal place codes. In *Nature neuroscience* 16 (3), pp. 264–266. DOI: 10.1038/nn.3329.

# ACKNOWLEDGEMENTS

# CURRICULUM VITAE
**Matthias Gumbert**

## EDUCATION

| | |
|---|---|
| *October 2017 – present* | **PhD in Systemic Neurosciences**<br>Graduate School of Systemic Neurosciences<br>Ludwig-Maximilians-University Munich, Germany<br>Supervisors:<br>Prof. Benedikt Grothe & Prof. Michael Myoga |
| *September 2014 – October 2016* | **MSc Cognitive Science**<br>University of Trento, Italy<br>Specialization: Cognitive Neuroscience |
| *October 2013 – September 2014* | **BSc Student in Psychology**<br>University of Innsbruck, Austria |
| *October 2010 – July 2013* | **BA German Studies**<br>Ludwig-Maximilians-University Munich, Germany<br>Specialization: Linguistics |

## SCHOLARSHIPS & AWARDS

| | |
|---|---|
| *May 2018* | **Merit Award**<br>University of Trento Trento, Italy |
| *March 2016 – June 2016* | **Thesis Research Abroad Scholarship**<br>University of Trento Trento, Italy |
| *March 2016* | **Munich Brain Course Award**<br>Ludwig-Maximilians-University Munich, Germany |
| *October 2015 – December 2015* | **Internship Scholarship**<br>University of Trento, Italy |
| *September 2014 – October 2016* | **Opera Universitaria Scholarship**<br>University of Trento, Italy |
| *August 2013* | **Travel Grant**<br>Ludwig-Maximilians-University Munich, Germany |

## CONFERENCE CONTRIBUTIONS

| | |
|---|---|
| *October 2017* | **Poster**<br>Meeting of the Society for the Neurobiology of Language Baltimore, USA |

| | |
|---|---|
| *July 2016* | **Poster** |
| | International Congress of Psychology Yokohama, Japan |
| *October 2015* | **Talk** |
| | European Congress of Psychology Milan, Italy |

## PUBLICATION

Meyer, L.* & **Gumbert, M.*** (2018). Synchronization of Electrophysiological Responses with Speech Benefits Syntactic Information Processing. *Journal of Cognitive Neuroscience.* *shared first authorship

## ADDITIONAL TRAINING AND RESEARCH EXPERIENCE

| | |
|---|---|
| *October 2017 – present* | **Guest Researcher** |
| | Max-Planck-Institute for Neurobiology Munich, Germany |
| *October 2015 – July 2016* | **Internship & Master's Research Training** |
| | Max-Planck-Institute for Cognitive and Brain Sciences Leipzig, Germany |
| | Supervisor: |
| | Dr. Lars Meyer |
| *January 2015 – July 2015* | **Lab Rotation** |
| | Center for Mind and Brain Sciences Trento, Italy |
| | Supervisors: |
| | Prof. Angelika Lingnau & Dr. Moritz Wurm |
| *February 2014 – May 2014* | **Internship** |
| | University of Innsbruck, Austria |
| | Supervisor: |
| | Prof. Pierre Sachse |

## METHODOLOGICAL SKILLS

| | |
|---|---|
| | *in-vivo* **chronic two-photon calcium imaging** |
| | **electroencephalography** |
| | **functional resonance imaging** |
| | **eye-tracking** |

## COMPUTING SKILLS

| | |
|---|---|
| *Operating systems* | **Windows, Mac, LINUX** |
| *Programming Languages* | **MATLAB, R, Python** |

## LANGUAGE SKILLS

| | |
|---|---|
| | **German (mother tongue)** |
| | **English (fluent)** |

# DECLARATION OF AUTHOR CONTRIBUTIONS

Experimental design: Matthias Gumbert, Michael Myoga, Benedikt Grothe

Setup design/assembly: Matthias Gumbert, Michael Myoga

Data acquisition: Matthias Gumbert

Data analysis: Matthias Gumbert, Michael Myoga

Data visualization: Matthias Gumbert

Supervision & project administration: Michael Myoga, Benedikt Grothe

Funding acquisition: Benedikt Grothe

Thesis writing: Matthias Gumbert

_____    _____

Date, place               Signature (Prof. Benedikt Grothe)

_____    _____

Date, place               Signature (Matthias Gumbert)